

CHAPTER IV

RESULTS AND DISCUSSIONS

In this study, the effects of the critical parameters on physical and piezoelectric properties were investigated. The characterization was conducted at the starting materials, the calcined powders and the sintered pellets of modified $\text{Bi}_{0.5}\text{Na}_{0.485}\text{La}_{0.005}\text{TiO}_3$ (BNLT). The analysis was done on the characterization techniques, i.e., PSD, XRD, SEM, dielectric properties and piezoelectric measurements. The results are presented in the following sections.

4.1 Particle Size Distribution

The modified $\text{Bi}_{0.5}\text{Na}_{0.485}\text{La}_{0.005}\text{TiO}_3$ (BNLT) powders were prepared by conventionally-mixed oxide method. The weight proportions of each oxides and carbonate in all batches are shown in Table 3.4-3.6 in Chapter III. A milling time of 24 hrs was used both before and after calcination step. The particle size analysis data of all substances, milled mixed oxides and milled calcined powders are shown in Table 4.1, Table 4.2-4.4 and Table 4.5-4.7, respectively. It was observed that the particle size of the as-received oxide and carbonate were categorized into two size ranges which are larger than 10 microns and smaller than 5 microns. The particle size of Bi_2O_3 , Na_2CO_3 and La_2O_3 exhibit a broaden size distribution, the mean particle diameter by volume are 30.96, 34.08 and 10.76 micron, respectively. And for TiO_2 , ZrO_2 , Nb_2O_5 and Fe_2O_3 are approximately 1.30, 2.77, 0.24 and 1.58 micron, respectively. The 24 hrs milling process improved the wide range of particle size of starting materials [5]. After milling process, the particles size of mixed oxides reduced to 2 – 6 microns of Zr-modified BNLT, 3-5 microns of Nb-modified BNLT and 9-14 microns of Fe-modified BNLT. After 24 hrs milling of calcined powders, the mean particle size were reduced into 0.5 – 2 microns.

Table 4.1 The particle size distribution of all starting materials

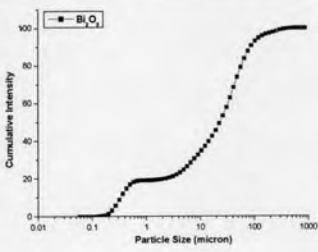
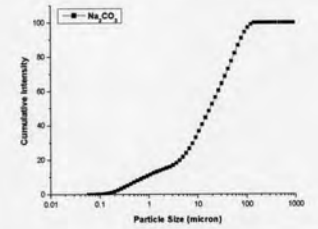
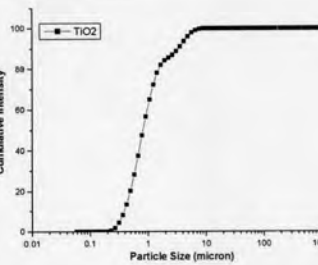
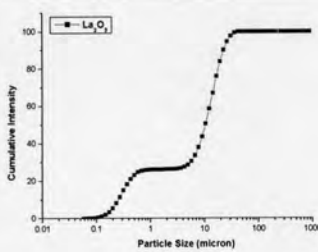
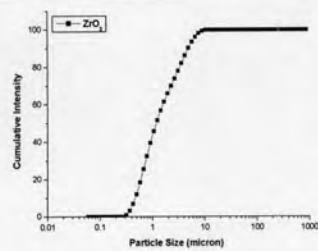
Particle size cumulative curve	Powder	Diameter (micron)	
		Volume Mean diameter	
	Bi ₂ O ₃	Volume Mean diameter	30.96 ± 0.85
		10% v ≤ diameter	0.33
		50% v ≤ diameter	21.14 ± 0.58
		90% v ≤ diameter	75.69 ± 1.54
	Na ₂ CO ₃	Volume Mean diameter	34.08 ± 0.64
		10% v ≤ diameter	1.05 ± 0.01
		50% v ≤ diameter	21.6 ± 0.68
		90% v ≤ diameter	85.76 ± 1.21
	TiO ₂	Volume Mean diameter	1.30
		10% v ≤ diameter	0.39
		50% v ≤ diameter	0.81
		90% v ≤ diameter	3.34 ± 0.01
	La ₂ O ₃	Volume Mean diameter	10.76 ± 0.08
		10% v ≤ diameter	0.25
		50% v ≤ diameter	10.34 ± 0.07
		90% v ≤ diameter	22.38 ± 0.15
	ZrO ₂	Volume Mean diameter	2.77 ± 0.50
		10% v ≤ diameter	0.57 ± 0.04
		50% v ≤ diameter	1.70 ± 0.04
		90% v ≤ diameter	6.59 ± 1.04

Table 4.1 (cont.)

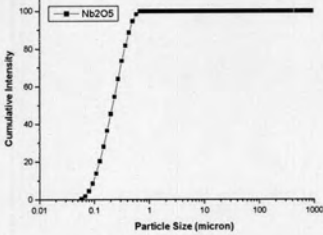
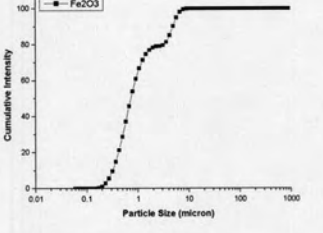
Particle size cumulative curve	Powder	Diameter (micron)	
	Nb ₂ O ₅	Volume Mean diameter	0.24
		10% v ≤ diameter	0.1
		50% v ≤ diameter	0.21
		90% v ≤ diameter	0.44
	Fe ₂ O ₃	Volume Mean diameter	1.58
		10% v ≤ diameter	0.32
		50% v ≤ diameter	0.73 ± 0.01
		90% v ≤ diameter	4.84 ± 0.01

Table 4.2 The particle size distribution of milled Zr-modified BNLT mixed-oxide powders

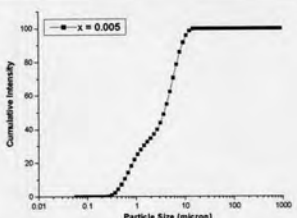
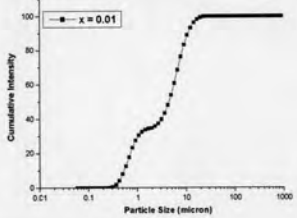
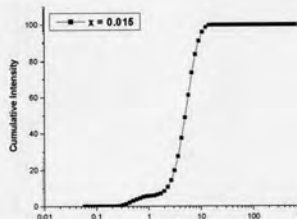
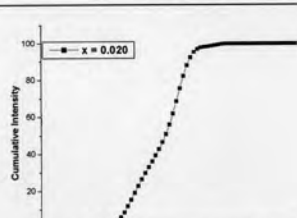
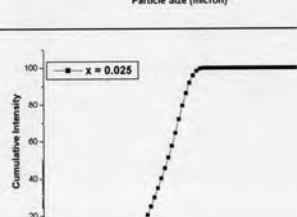
Particle size cumulative curve	Powder	Diameter (micron)	
		Volume Mean diameter	
	x = 0.005	Volume Mean diameter	4.00 ± 0.08
		10% v ≤ diameter	0.56
		50% v ≤ diameter	3.61 ± 0.08
		90% v ≤ diameter	8.35 ± 0.19
	x = 0.010	Volume Mean diameter	4.88 ± 0.09
		10% v ≤ diameter	0.50 ± 0.03
		50% v ≤ diameter	4.30 ± 0.28
		90% v ≤ diameter	10.71 ± 0.37
	x = 0.015	Volume Mean diameter	6.07 ± 0.03
		10% v ≤ diameter	2.59 ± 0.09
		50% v ≤ diameter	5.77 ± 0.03
		90% v ≤ diameter	10.07 ± 0.19
	x = 0.020	Volume Mean diameter	3.50 ± 0.09
		10% v ≤ diameter	0.45 ± 0.01
		50% v ≤ diameter	2.58 ± 0.01
		90% v ≤ diameter	7 ± 0.07
	x = 0.025	Volume Mean diameter	2.75 ± 0.10
		10% v ≤ diameter	0.63 ± 0.01
		50% v ≤ diameter	2.32 ± 0.13
		90% v ≤ diameter	5.53 ± 0.16

Table 4.3 The particle size distribution of milled Nb-modified BNLT mixed-oxide powders

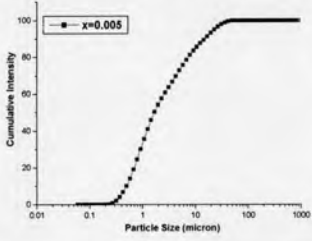
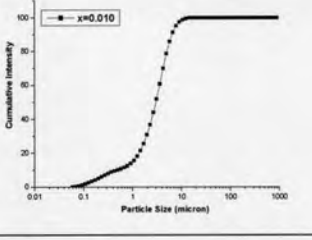
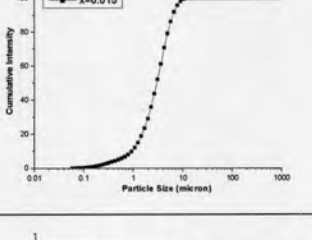
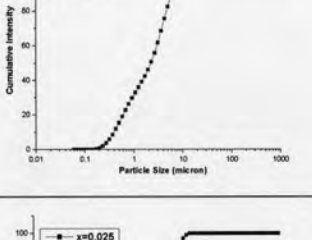
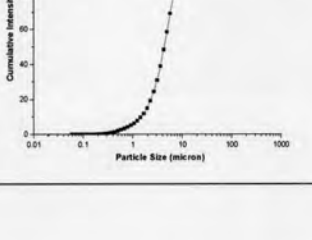
Particle size cumulative curve	Powder	Diameter (micron)	
		Volume Mean diameter	
	x = 0.005	Volume Mean diameter	4.94 ± 0.02
		10% v ≤ diameter	0.49 ± 0.01
		50% v ≤ diameter	1.63 ± 0.04
		90% v ≤ diameter	14.66 ± 0.05
	x = 0.010	Volume Mean diameter	3.43 ± 0.14
		10% v ≤ diameter	0.50 ± 0.04
		50% v ≤ diameter	2.95 ± 0.02
		90% v ≤ diameter	6.69 ± 0.44
	x = 0.015	Volume Mean diameter	3.82 ± 0.07
		10% v ≤ diameter	1.12 ± 0.07
		50% v ≤ diameter	3.47 ± 0.05
		90% v ≤ diameter	7.00 ± 0.07
	x = 0.020	Volume Mean diameter	3.19 ± 0.04
		10% v ≤ diameter	1.16 ± 0.06
		50% v ≤ diameter	3.24 ± 0.07
		90% v ≤ diameter	6.25 ± 0.16
	x = 0.025	Volume Mean diameter	4.58 ± 0.05
		10% v ≤ diameter	1.36 ± 0.17
		50% v ≤ diameter	4.23 ± 0.07
		90% v ≤ diameter	8.25 ± 0.15

Table 4.4 The particle size distribution of milled Fe-modified BNL mixed-oxide powders

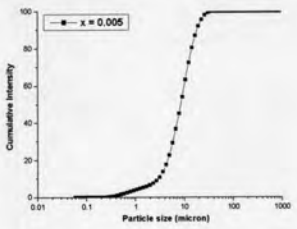
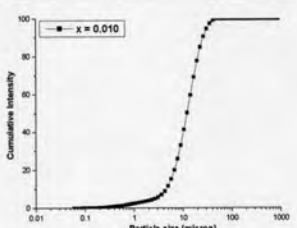
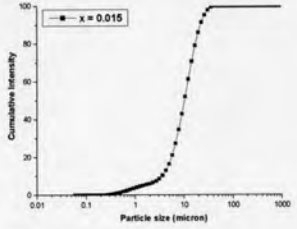
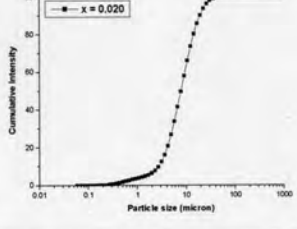
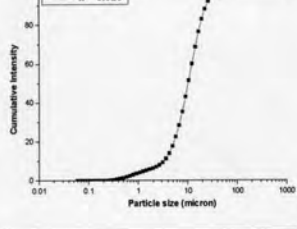
Particle size cumulative curve	Powder	Diameter (micron)	
		Volume Mean diameter	
	x = 0.005	Volume Mean diameter	9.14 ± 0.42
		10% v ≤ diameter	2.71 ± 0.18
		50% v ≤ diameter	8.03 ± 0.33
		90% v ≤ diameter	17.21 ± 0.74
	x = 0.010	Volume Mean diameter	13.69 ± 0.14
		10% v ≤ diameter	4.46 ± 0.02
		50% v ≤ diameter	12.01 ± 0.12
		90% v ≤ diameter	25.14 ± 0.29
	x = 0.015	Volume Mean diameter	10.49 ± 0.94
		10% v ≤ diameter	3.43 ± 0.16
		50% v ≤ diameter	9.48 ± 0.62
		90% v ≤ diameter	19.07 ± 2.21
	x = 0.020	Volume Mean diameter	9.69 ± 0.07
		10% v ≤ diameter	2.71 ± 0.01
		50% v ≤ diameter	7.76 ± 0.03
		90% v ≤ diameter	19.28 ± 0.21
	x = 0.025	Volume Mean diameter	12.41 ± 0.02
		10% v ≤ diameter	3.32 ± 0.05
		50% v ≤ diameter	10.25 ± 0.05
		90% v ≤ diameter	23.91 ± 0.07

Table 4.5 The particle size distribution of milled-calcined Zr-modified BNLTP powders

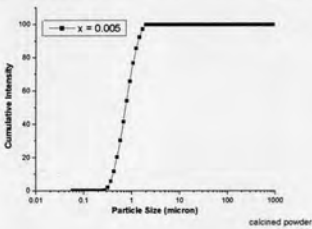
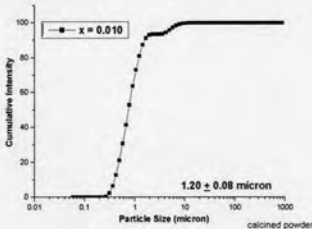
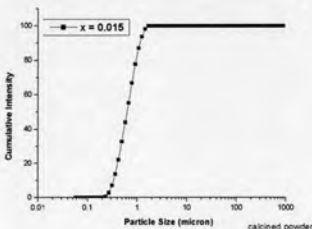
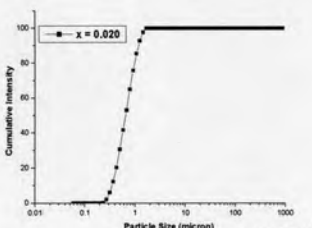
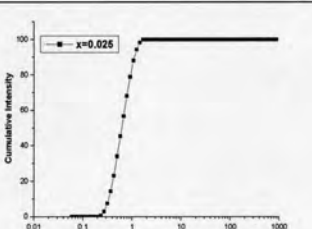
Particle size cumulative curve	Powder	Diameter (micron)	
		Volume Mean diameter	
	x = 0.005	Volume Mean diameter	0.81 ± 0.01
		10% v ≤ diameter	0.40 ± 0.01
		50% v ≤ diameter	0.74 ± 0.01
		90% v ≤ diameter	1.34 ± 0.02
	x = 0.010	Volume Mean diameter	1.20 ± 0.08
		10% v ≤ diameter	0.39
		50% v ≤ diameter	0.75 ± 0.01
		90% v ≤ diameter	1.66 ± 0.12
	x = 0.015	Volume Mean diameter	0.69
		10% v ≤ diameter	0.34
		50% v ≤ diameter	0.63
		90% v ≤ diameter	1.13
	x = 0.020	Volume Mean diameter	0.70 ± 0.01
		10% v ≤ diameter	0.35
		50% v ≤ diameter	0.64 ± 0.01
		90% v ≤ diameter	1.16 ± 0.01
	x = 0.025	Volume Mean diameter	0.67
		10% v ≤ diameter	0.33
		50% v ≤ diameter	0.61
		90% v ≤ diameter	1.11 ± 0.01

Table 4.6 The particle size distribution of milled-calcined Nb-modified BNLTL powders

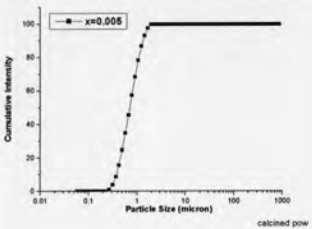
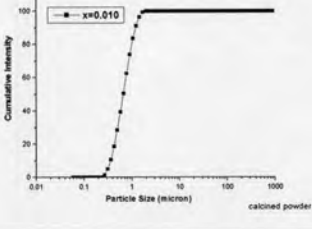
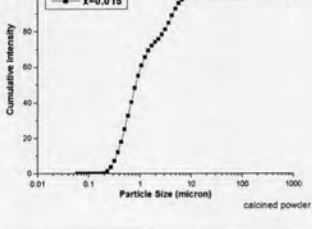
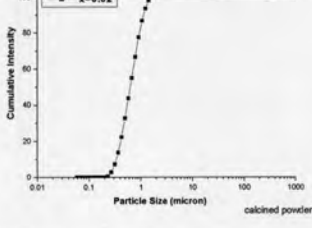
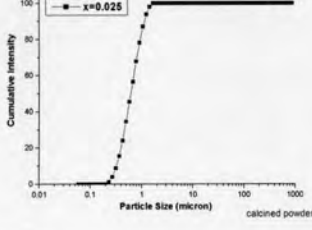
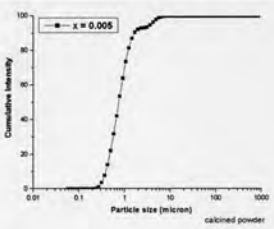
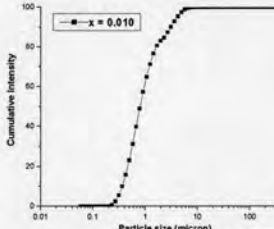
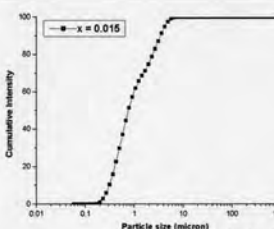
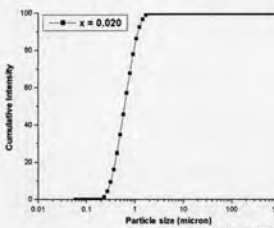
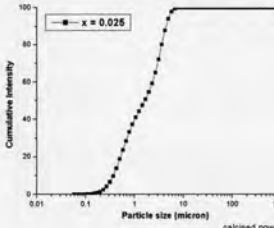
Particle size cumulative curve	Powder	Diameter (micron)	
		Volume Mean diameter	
	x = 0.005	Volume Mean diameter	0.79
		10% v ≤ diameter	0.38 ± 0.01
		50% v ≤ diameter	0.71
		90% v ≤ diameter	1.34 ± 0.01
	x = 0.010	Volume Mean diameter	0.72 ± 0.01
		10% v ≤ diameter	0.36
		50% v ≤ diameter	0.66 ± 0.01
		90% v ≤ diameter	1.19 ± 0.02
	x = 0.015	Volume Mean diameter	1.59 ± 0.02
		10% v ≤ diameter	0.34
		50% v ≤ diameter	0.80 ± 0.01
		90% v ≤ diameter	4.32 ± 0.03
	x = 0.020	Volume Mean diameter	0.69
		10% v ≤ diameter	0.33 ± 0.01
		50% v ≤ diameter	0.63
		90% v ≤ diameter	1.13 ± 0.01
	x = 0.025	Volume Mean diameter	0.68 ± 0.01
		10% v ≤ diameter	0.32 ± 0.01
		50% v ≤ diameter	0.62 ± 0.01
		90% v ≤ diameter	1.14 ± 0.01

Table 4.7 The particle size distribution of milled-calcined Fe-modified BNLT powders

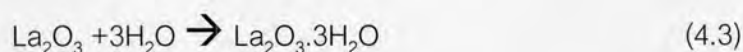
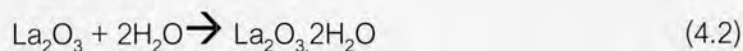
Particle size cumulative curve	Powder	Diameter (micron)	
		Volume Mean diameter	
	x = 0.005	Volume Mean diameter	1.02 ± 0.02
		10% v ≤ diameter	0.40 ± 0.01
		50% v ≤ diameter	0.75
		90% v ≤ diameter	1.57 ± 0.05
	x = 0.010	Volume Mean diameter	1.26 ± 0.02
		10% v ≤ diameter	0.37
		50% v ≤ diameter	0.80
		90% v ≤ diameter	1.57 ± 0.05
	x = 0.015	Volume Mean diameter	1.58 ± 0.04
		10% v ≤ diameter	0.36 ± 0.01
		50% v ≤ diameter	0.86 ± 0.04
		90% v ≤ diameter	4.06 ± 0.09
	x = 0.020	Volume Mean diameter	0.79 ± 0.01
		10% v ≤ diameter	0.37
		50% v ≤ diameter	0.71
		90% v ≤ diameter	1.34 ± 0.01
	x = 0.025	Volume Mean diameter	2.06 ± 0.01
		10% v ≤ diameter	0.37
		50% v ≤ diameter	1.61 ± 0.01
		90% v ≤ diameter	4.39 ± 0.01

The conclusions of this section are presented in this following part. The broaden particle size distribution of mixed oxides and carbonate powder can improve by milling process. 24 H milling time of mixed oxides and carbonate powder can reduce the wide range of particle size of starting substances. For calcined powders, the agglomeration particles were also reduced by milling process. After milling process, the obtained powders

are easier to form into pellet than the as-received calcined one. So the milling step in the both of before and after calcination process is the necessary step.

4.2 Thermal Analysis of starting materials

Na_2CO_3 and La_2O_3 were investigated the percentage of weight losses in the range of room temperature (30°C) up to 1300°C . The simultaneously thermal analysis technique was selected for investigation. First, Na_2CO_3 was one of the starting materials which hygroscopic or easily adsorb the water molecule on to the particle surface [41]. The TG and DTG curves of Na_2CO_3 (Fig. 4.1) exhibit two steps of decompositions. The first step presents at approximately 100°C which is the dehydration of surface water [42]. The weight loss in this step is approximately 6%. And the second step presents at 850°C which is the decomposition of carbonate ($\text{Na}_2\text{CO}_{3(s)} \rightarrow \text{Na}_2\text{O}_{(s)} + \text{CO}_{2(g)}$) [42]. The total weight loss of as-received Na_2CO_3 is approximately 55%. La_2O_3 is very hygroscopic at ambient temperature [41]. The La_2O_3 may absorb one or two molecules of water by partial hydrolysis as shown in reactions (4.1) and (4.2), or by total hydrolysis as shown in reaction (4.3) [5].



The TG and DTG curves of La_2O_3 (Fig. 4.2) show three steps of weight losses at temperature of approximately 370 , 500 and 700°C , respectively. The three steps of losses are from the decompositions of H_2O in three equations above. The weight losses of the above temperatures are 9%, 4% and 2%, respectively. The total weight loss of as-received La_2O_3 is approximately 15%.

The conclusion for this section is mainly in the thermal characterization of Na_2CO_3 and La_2O_3 which are hygroscopic substances. So in the BNLT powder preparation step, weighing formula both of Na_2CO_3 and La_2O_3 have to include the weight loss from surface water and molecular water, in order to balance the stoichiometry.

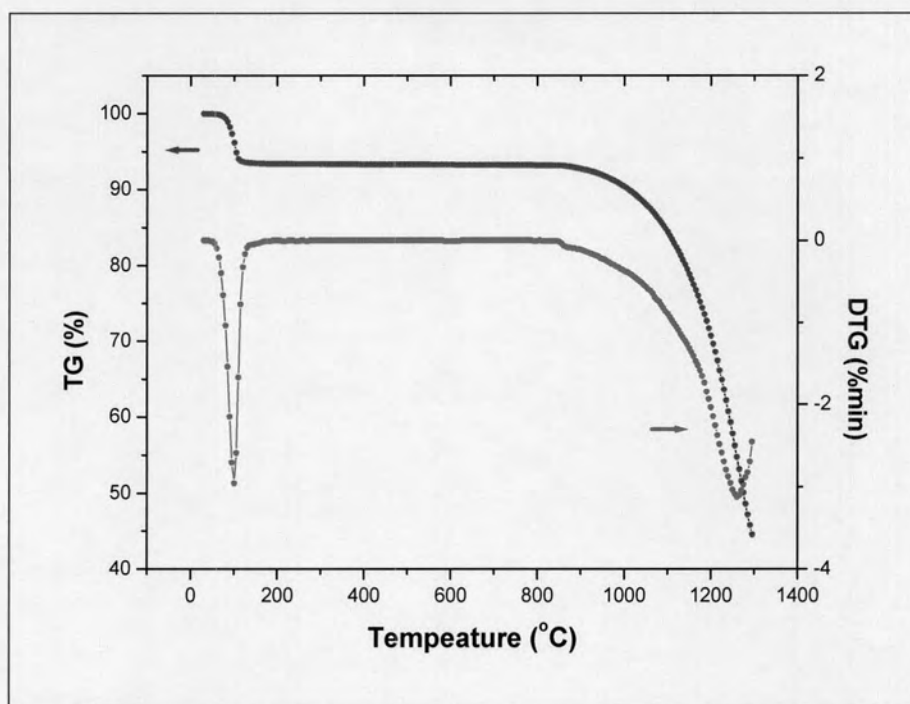


Fig. 4.1 The TG and DTG curves of sodium bicarbonate (Na_2CO_3)

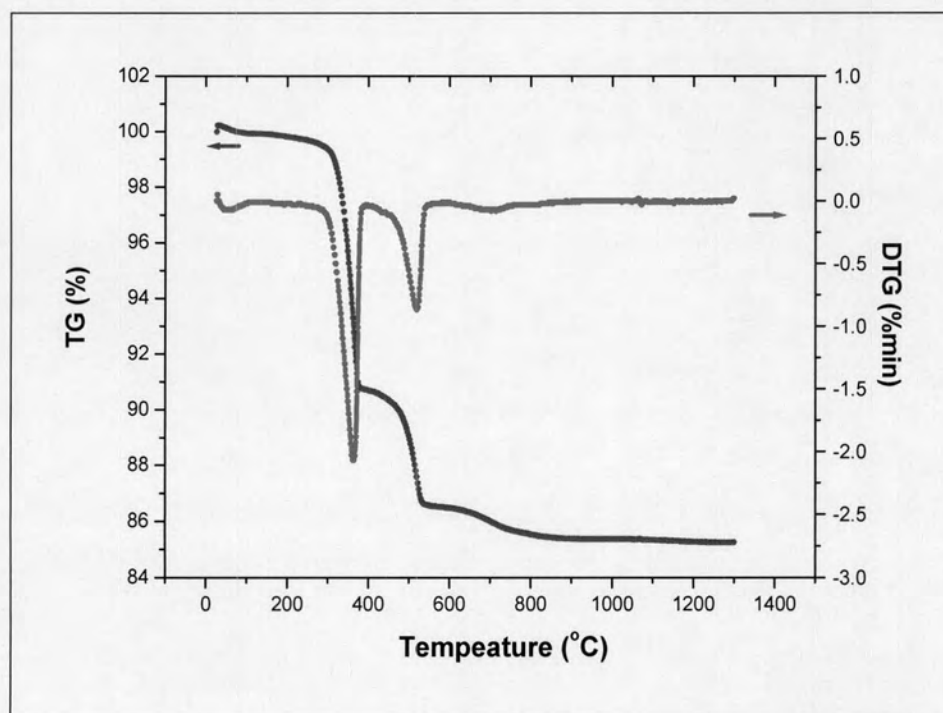


Fig. 4.2 The TG and DTG curves of lanthanum oxide (La_2O_3)

4.3 Phase development by X-ray diffraction analysis

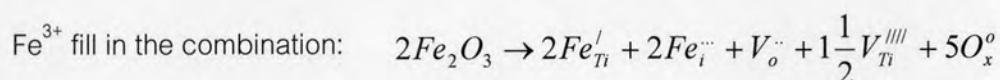
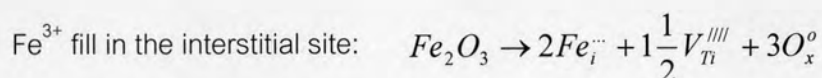
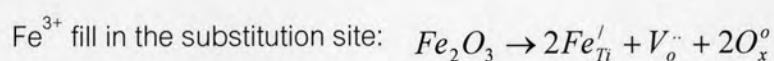
Fig. 4.3 – 4.5 is the comparison of XRD patterns of Zr-BNLT, Nb-BNLT and Fe-BNLT powders calcined at 750, 800 and 850 °C for 2 h. After calcination at 800 °C for 2 h, a pure perovskite BNT phase was obtained (indicated with JCPDS card No. 36-0340; $\text{Bi}_{0.5}\text{Na}_{0.5}\text{TiO}_3$) [45], as indicated by the presence of its characteristic diffraction pattern. It should be noted that this phase started to form BNT at 750 °C for 2 h; however the relative intensities of the BNT peaks at 800 °C are higher than at 750 °C, indicating that the calcinations at 800 °C rendered more complete crystallinity of the BNT phase [5].

Fig. 4.6 shows the XRD patterns of sintered Zr-BNLT at various sintering temperatures and Zr^{4+} concentrations. The silicon powders were used as an internal standard for calibration. The lattice distortion of Zr-BNLT was observed from all of peaks shift to lower 2-theta. The lattice distances (a_r) of the modified BNLT compounds increased with an increase in an addition of zirconium substitutions and tendency to stable at the Zr^{4+} content up to 1 at% shown in Table 4.8 and Fig. 4.9. The expansion of lattice distance can also explain by the substituent radii. Zr^{4+} has larger ionic radius (0.72 Å) than Ti^{4+} (0.61 Å) [43] causing an increase in the lattice distance [17].

The XRD patterns of sintered Nb-BNLT are shown in Fig. 4.7. The high sintering temperatures (≥ 1100 °C) broke down the single BNT perovskite phase into $\text{Bi}_{0.5}\text{Na}_{0.5}\text{TiO}_3$ (36-0340), $\text{Na}_{0.5}\text{Bi}_{8.5}\text{Ti}_7\text{O}_{27}$ (32-1044) and Ti_6O_{11} (18-1401), so that the suitable temperature in this study should be 1050 °C for 2 hrs. The lattice parameters are summarized in Table 4.9 and Fig. 4.10. The lattice distances (a_r) of the Nb-BNLT pellets increased with an increase in an addition of niobium substitutions same as Zr-BNLT because Nb^{5+} has 0.64 Å ionic radius [43] which larger than Ti^{4+} until the concentration of Nb is reached 2.0 at% the lattice distance is stable.

The XRD patterns of sintered Fe-BNLT were shown in Fig. 4.8 and the lattice parameters were summarized in Table 4.10 and Fig. 4.11. The opposite tendency was presented in Fe-BNLT, the increasing in Fe concentrations were presented the smaller lattice

distance. Fe^{3+} has an 0.65 Å of ionic radius [43] which was larger than Ti^{4+} (same as Zr^{4+} and Nb^{5+}), however, due to doping of the lower oxidation state element is created the oxygen vacancies which might cause the movement of the atoms closer together than the pure BNLT that might be the reason of negative tendency [17]. The possible defect equations of Fe-BNLT are shown in the following below [25]:



The conclusion of this section is the 800 °C for 2 h calcined BNLT powders were a pure perovskite phase detected by XRD. For Nb-BNLT sintering temperature of higher than 1050°C, the perovskite phase dissociate into 3 phases of $Bi_{0.5}Na_{0.5}TiO_3$, $Na_{0.5}Bi_{8.5}Ti_7O_{27}$ and Ti_6O_{11} . The lattice constant of Zr-BNLT and Nb-BNLT increase with an increase in an addition of substitutions. On the contrary, with an increase in Fe concentration in BNLT system, the lattice constant of Fe-BNLT pellet was decrease.

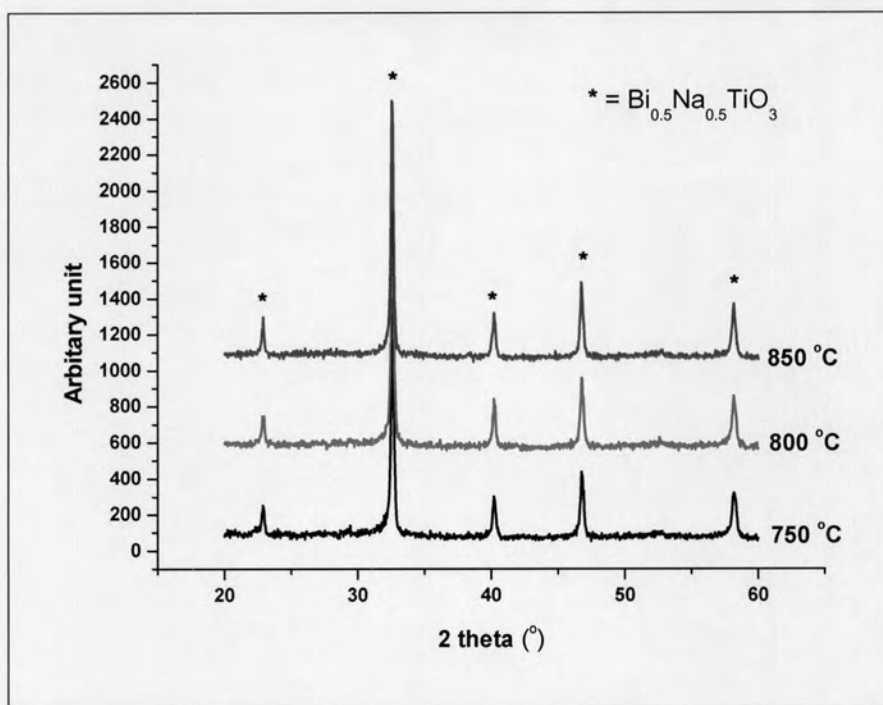


Fig. 4.3 X-ray diffraction patterns of $\text{Bi}_{0.5}\text{Na}_{0.485}\text{La}_{0.005}\text{Zr}_{0.005}\text{Ti}_{0.995}\text{O}_3$ at three calcination temperatures

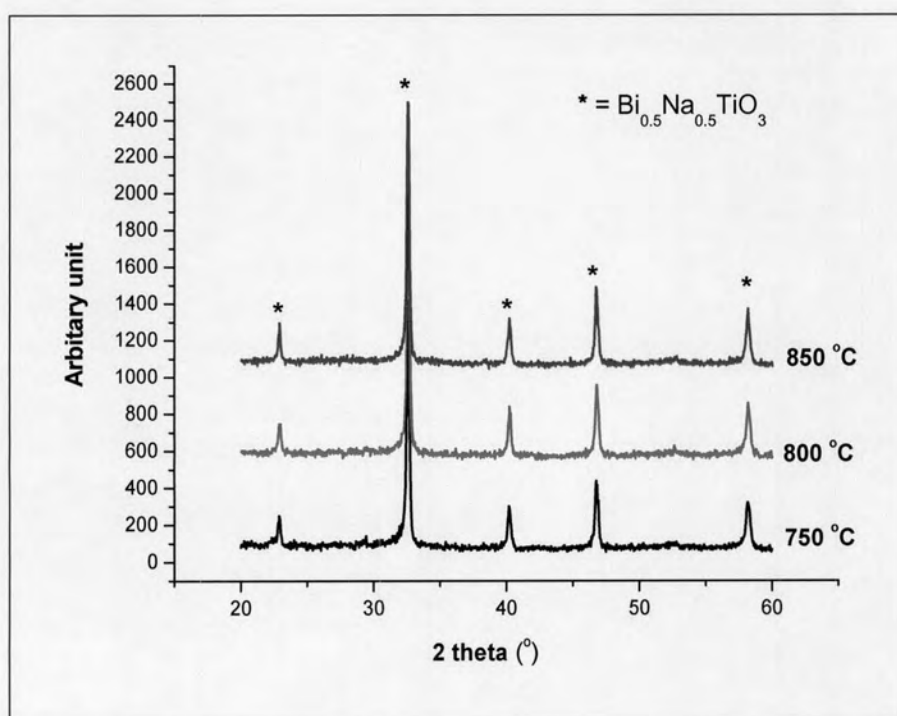


Fig. 4.4 X-ray diffraction patterns of $\text{Bi}_{0.5}\text{Na}_{0.485}\text{La}_{0.005}\text{Nb}_{0.005}\text{Ti}_{0.994}\text{O}_3$ at three calcination temperatures

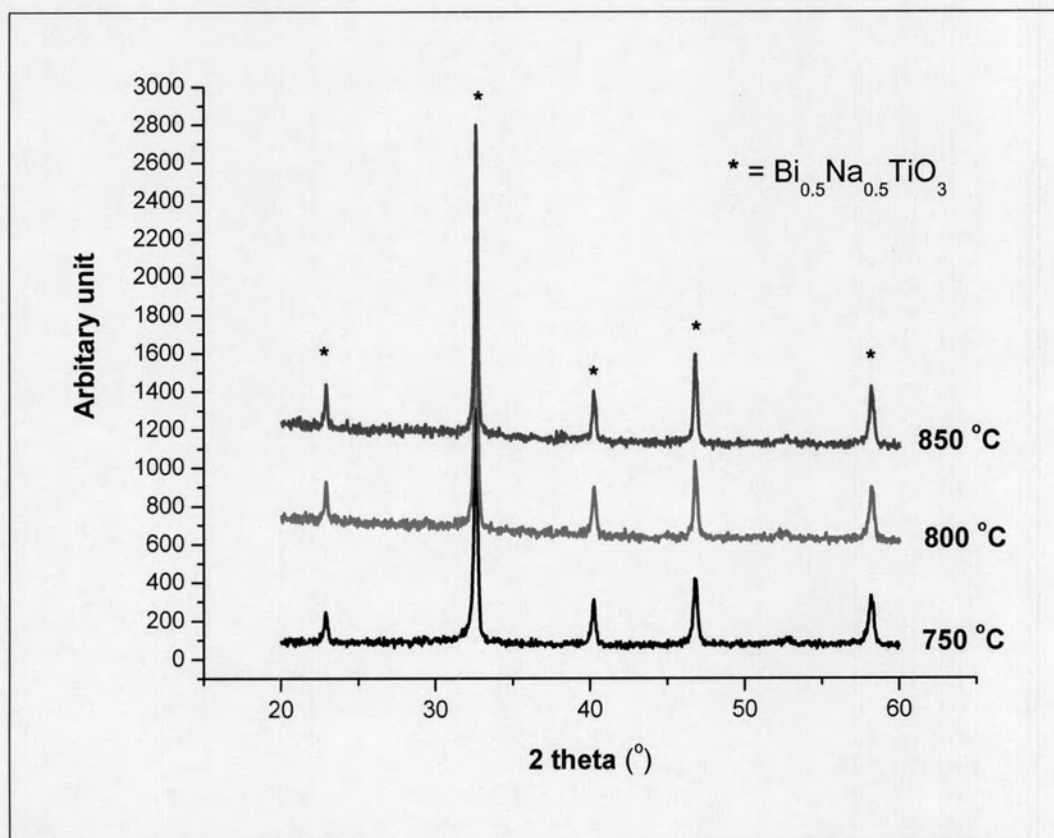


Fig. 4.5 X-ray diffraction patterns of $\text{Bi}_{0.5}\text{Na}_{0.485}\text{La}_{0.005}\text{Fe}_{0.005}\text{Ti}_{0.996}\text{O}_3$ at three calcination temperatures

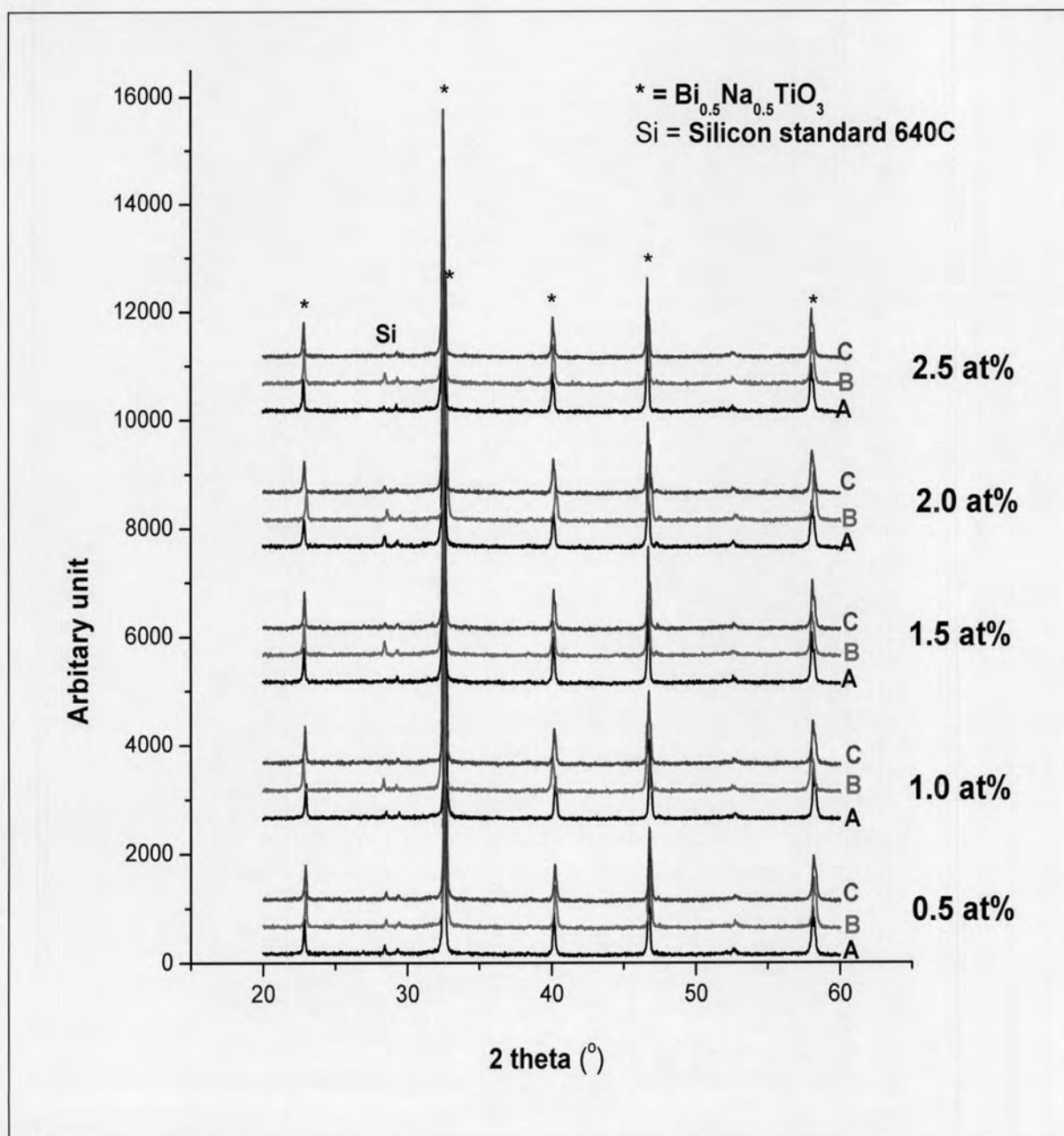


Fig. 4.6 X-ray diffraction patterns of $\text{Bi}_{0.5}\text{Na}_{0.485}\text{La}_{0.005}\text{Zr}_{0.005}\text{Ti}_{0.995}\text{O}_3$ after sintering at various sintering temperature; A = 1050, B = 1100 and C = 1150 °C.

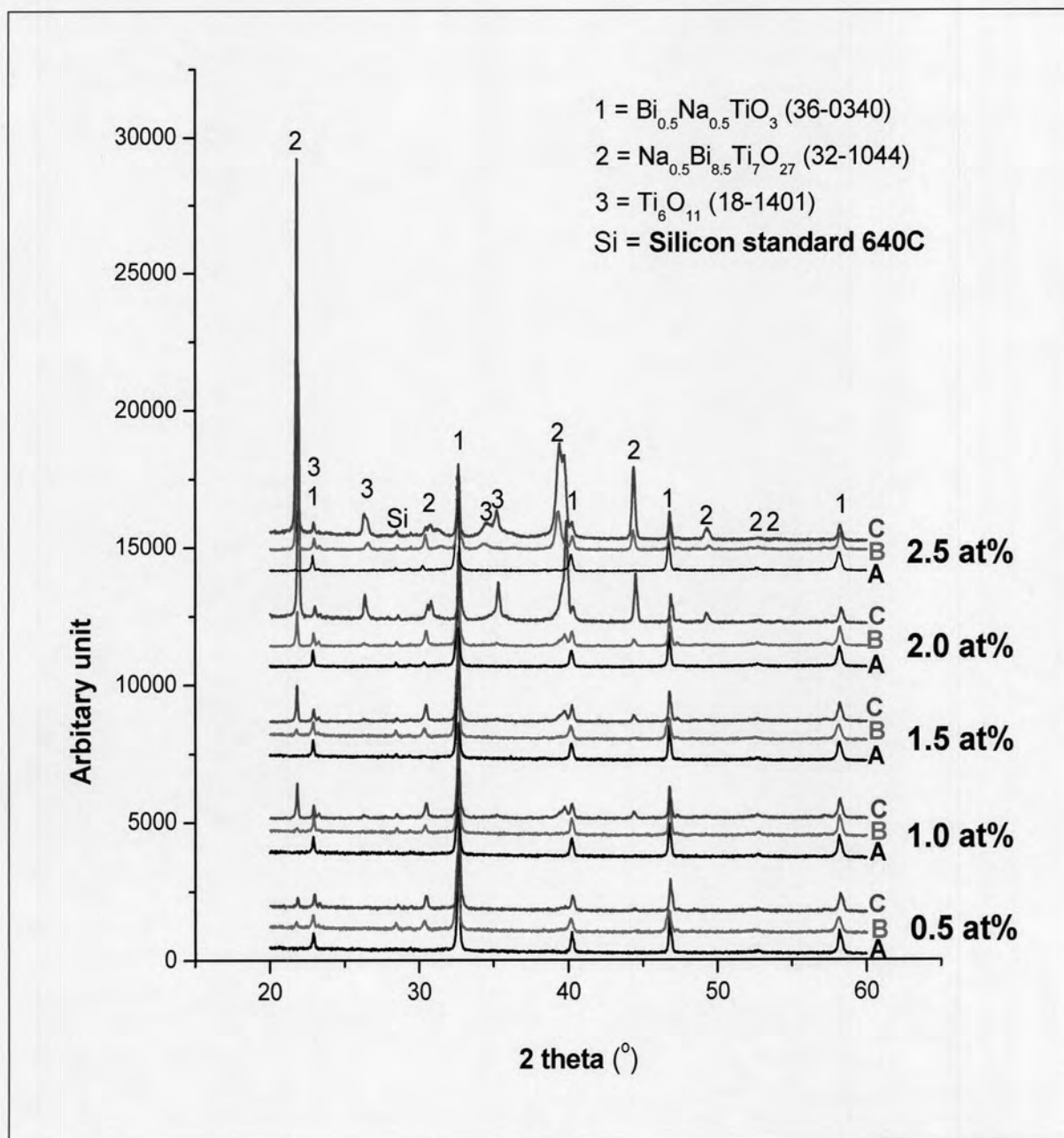


Fig. 4.7 X-ray diffraction patterns of $\text{Bi}_{0.5}\text{Na}_{0.485}\text{La}_{0.005}\text{Nb}_{0.005}\text{Ti}_{0.994}\text{O}_3$ after sintering at various sintering temperature; A = 1050, B = 1100 and C = 1150 °C.

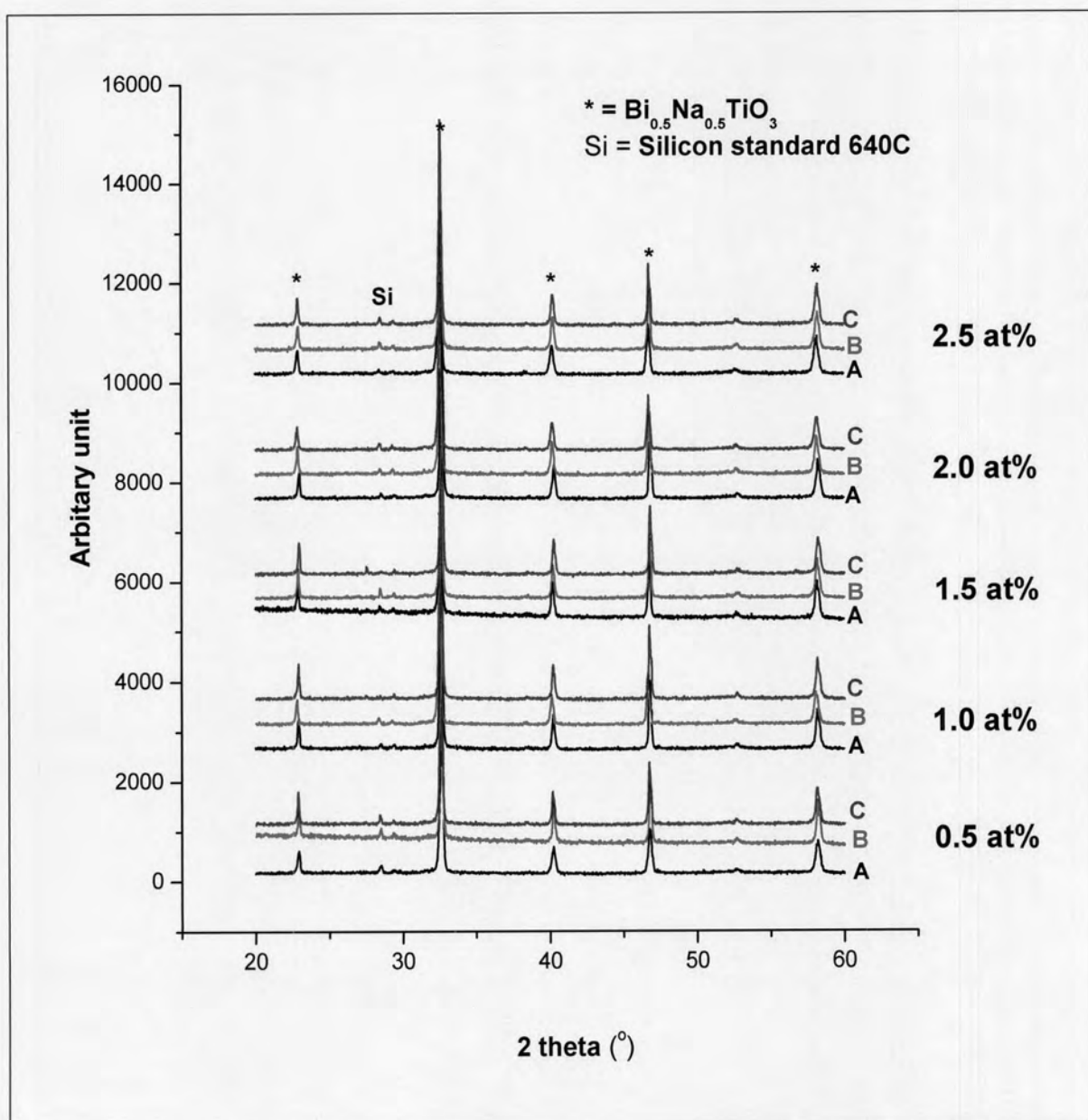


Fig. 4.8 X-ray diffraction patterns of $\text{Bi}_{0.5}\text{Na}_{0.485}\text{La}_{0.005}\text{Fe}_{0.005}\text{Ti}_{0.996}\text{O}_3$ after sintering at various sintering temperature; A = 1050, B = 1100 and C = 1150 °C.

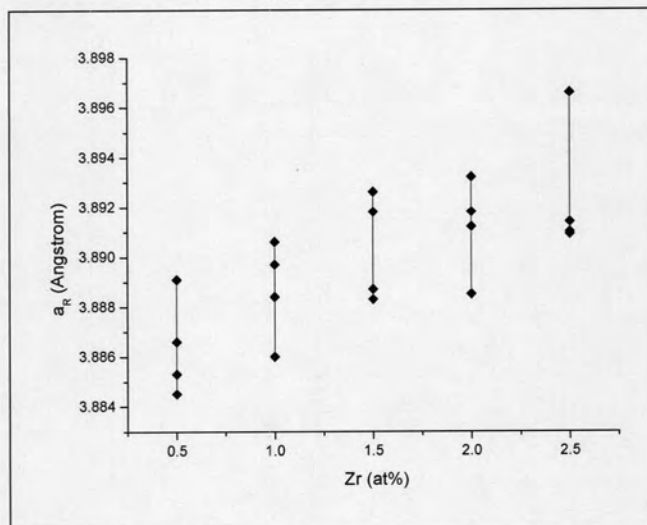


Fig. 4.9 The lattice parameter of Zr-modified BNLTL of rhombohedral structure

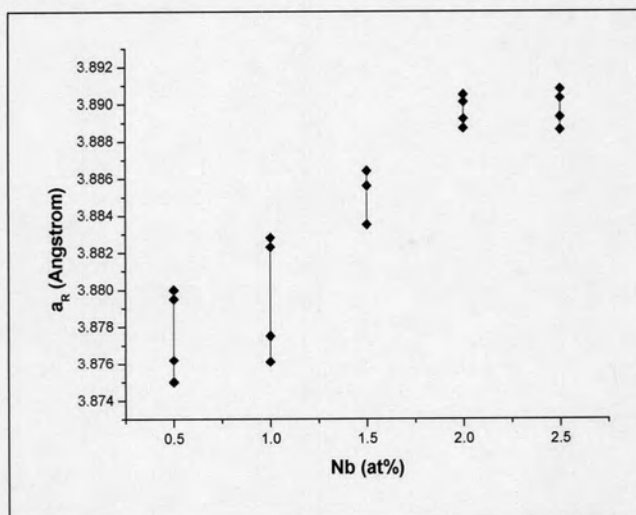


Fig. 4.10 The lattice parameter of Nb-modified BNLTL of rhombohedral structure

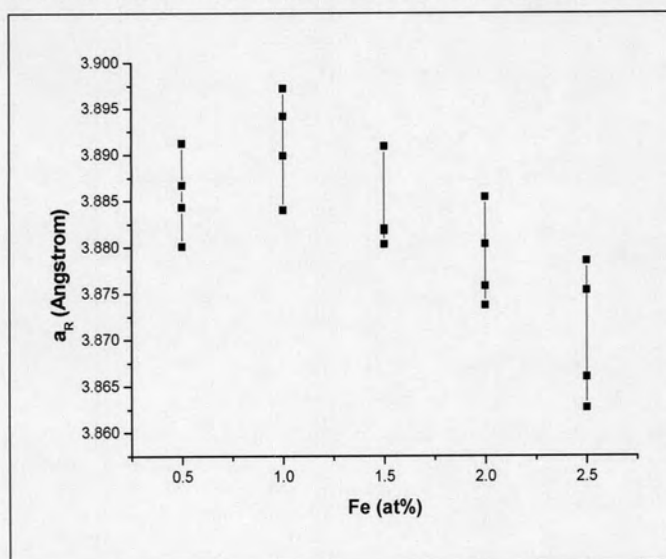


Fig. 4.11 The lattice parameter of Fe-modified BNLTL of rhombohedral structure

Table 4.8 Lattice parameters of $\text{Bi}_{0.5}\text{Na}_{0.485}\text{La}_{0.005}\text{Zr}_x\text{Ti}_{(1-x)}\text{O}_3$

x	Structure	a_R		angle	
		Average	SD	Average	SD
0.5	Rhombohedral	3.8887	0.0017	89.9003	0.0838
1.0	Rhombohedral	3.8864	0.0017	89.9615	0.0523
1.5	Rhombohedral	3.8904	0.0019	89.9303	0.0804
2.0	Rhombohedral	3.8912	0.0017	89.9805	0.0551
2.5	Rhombohedral	3.8925	0.0024	89.9325	0.0677

Table 4.9 Lattice parameters of $\text{Bi}_{0.5}\text{Na}_{0.485}\text{La}_{0.005}\text{Nb}_x\text{Ti}_{(1-(5/4)x)}\text{O}_3$

x	Structure	a_R		angle	
		Average	SD	Average	SD
0.5	Rhombohedral	3.8813	0.0119	90.0758	0.2304
1.0	Rhombohedral	3.8832	0.0078	89.9860	0.2490
1.5	Rhombohedral	3.8875	0.0048	89.8588	0.0899
2.0	Rhombohedral	3.8721	0.0344	89.6068	0.1062
2.5	Rhombohedral	3.8898	0.0010	89.4425	0.7376

Table 4.10 Lattice parameters of $\text{Bi}_{0.5}\text{Na}_{0.485}\text{La}_{0.005}\text{Fe}_x\text{Ti}_{(1-(3/4)x)}\text{O}_3$

x	Structure	a_R		angle	
		Average	SD	Average	SD
0.5	Rhombohedral	3.8856	0.0046	89.9435	0.0983
1.0	Rhombohedral	3.8913	0.0057	89.8975	0.1525
1.5	Rhombohedral	3.8838	0.0048	89.9902	0.0615
2.0	Rhombohedral	3.8788	0.0052	90.1280	0.1606
2.5	Rhombohedral	3.8906	0.0236	89.6925	0.6630

4.4 Physical properties

4.4.1 Volume shrinkage

After sintering process, ceramic particles were move to close together in order to reduce the surface energy. At high temperature, the sample volume gradually decreases due to the shrinkage occurring [44]. The volume shrinkage of three modified BNLT-based at various temperature were measured by dimensional measurement. The volume shrinkage of sintered Zr-BNLT specimens was in the range of 30 - 40% (Fig. 4.12). The tendency of volume shrinkage was increased with increasing temperature. After the sintering temperature reach 1100 °C the volume shrinkage decreased due to over-firing temperature. The maximum volume shrinkage of Zr-BNLT pellets obtained at 1100 °C of sintering temperature. The volume shrinkages of Nb-BNLT specimens sintered at 1050°C were approximately 26 - 30% (Fig. 4.13). The volume shrinkage of Nb-BNLT which sintered at 1100 and 1150 °C are approximately 32 – 38 %. For the Fe-BNLT, the volume shrinkage was around 32 - 34% (Fig. 4.14) at 1100°C which was suitable sintering temperature. The 1150 °C of sintering temperature of Fe-BNLT obtained lower volume shrinkage that might be over-fired of sintering temperature.

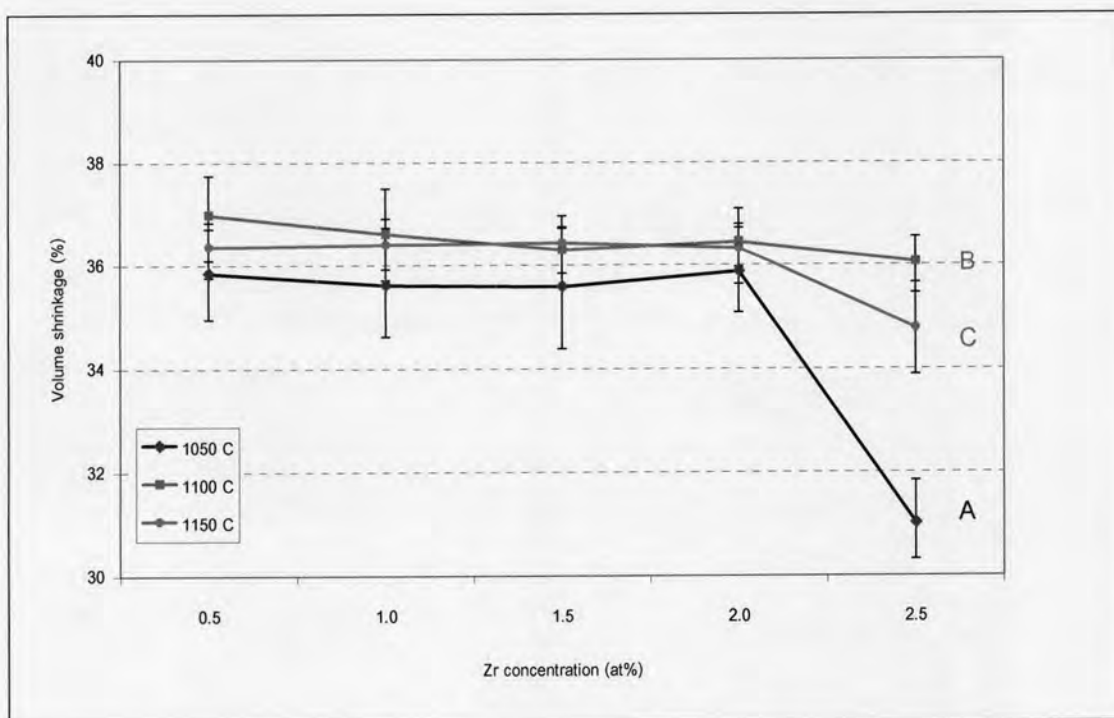


Fig. 4.12 The volume shrinkage of $\text{Bi}_{0.5}\text{Na}_{0.485}\text{La}_{0.005}\text{Zr}_x\text{Ti}_{(1-x)}\text{O}_3$ at 3 sintering temperatures; A = 1050°C, B = 1100 °C and C = 1150°C

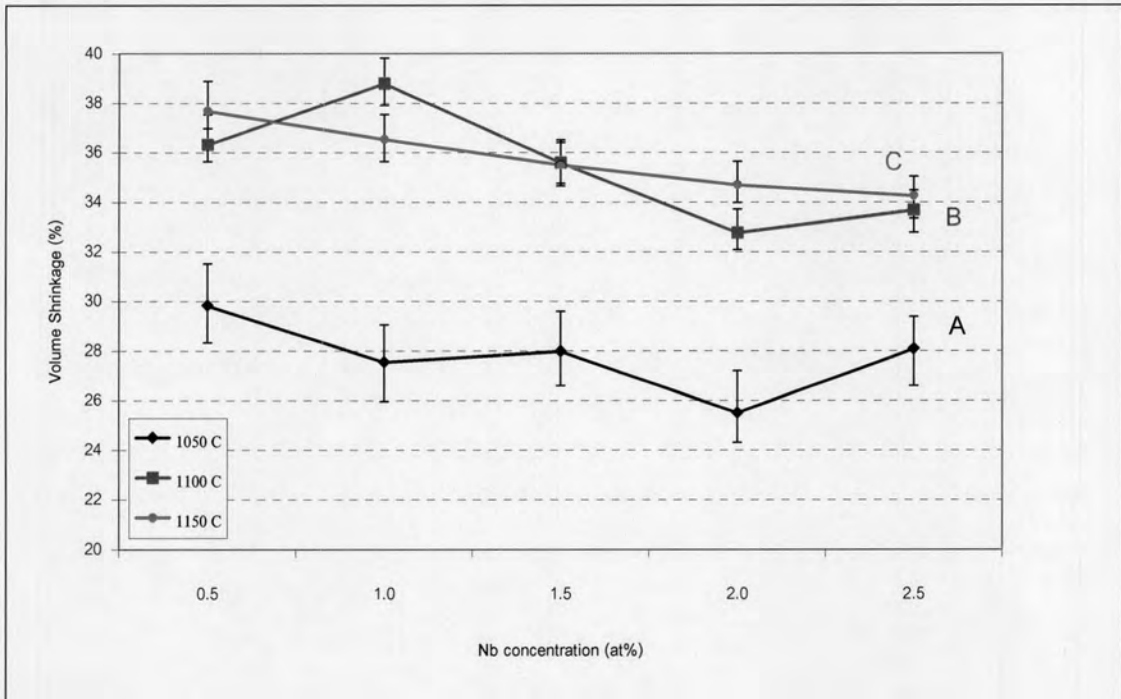


Fig. 4.13 The volume shrinkage of $\text{Bi}_{0.5}\text{Na}_{0.485}\text{La}_{0.005}\text{Nb}_x\text{Ti}_{(1-(3/4)x)}\text{O}_3$ at 3 sintering temperatures; A = 1050°C, B = 1100 °C and C = 1150°C

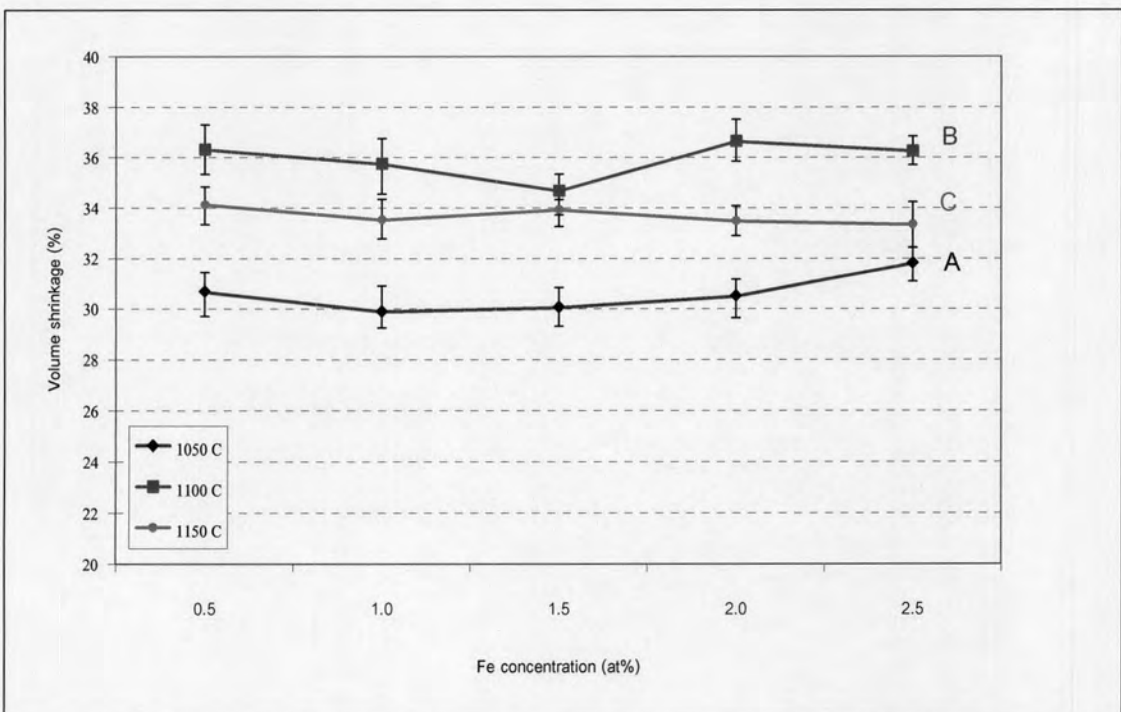


Fig. 4.14 The volume shrinkage of $\text{Bi}_{0.5}\text{Na}_{0.485}\text{La}_{0.005}\text{Fe}_x\text{Ti}_{(1-(3/4)x)}\text{O}_3$ at 3 sintering temperatures; A = 1050°C, B = 1100 °C and C = 1150°C

4.4.2 Theoretical density

The theoretical density of all samples were performed both of green and fired densities by calculating the relative between the measuring density and x-ray density [45]. The green and fired densities were summarized in Table 4.11- 4.12. The densities of green pellets of all samples could achieve at approximately 60% of theoretical density. The density of sintered Zr-BNLT obtained 97% of theoretical density at 1100°C for 2 h. For Nb-BNLT obtained 90 - 94% theoretical density because of low sintering temperature (1050 °C for 2 h). The high sintering temperature (≥ 1100 °C) broke down the single perovskite phase of BNT (reported in XRD section). The %theoretical density of Fe-BNLTs reached to 98% at 1100 °C for 2 h of sintering temperature.

Table 4.11 %Theoretical density of green samples of modified BNLT

Composition	Measured density (g/cm ³)	Theoretical density (g/cm ³)	%Theoretical density
BNLT+Zr 0.5 at%	3.765	6.020	63
BNLT+Zr 1.0 at%	3.665	6.026	61
BNLT+Zr 1.5 at%	3.757	6.021	62
BNLT+Zr 2.0 at%	3.753	6.017	62
BNLT+Zr 2.5 at%	3.744	6.021	62
BNLT+Nb 0.5 at%	3.729	6.346	59
BNLT+Nb 1.0 at%	3.700	6.319	59
BNLT+Nb 1.5 at%	3.845	6.321	61
BNLT+Nb 2.0 at%	3.963	6.381	62
BNLT+Nb 2.5 at%	3.889	6.346	61
BNLT+Fe 0.5 at%	3.725	6.034	62
BNLT+Fe 1.0 at%	3.692	6.025	61
BNLT+Fe 1.5 at%	3.743	6.048	62
BNLT+Fe 2.0 at%	3.750	6.089	62
BNLT+Fe 2.5 at%	3.770	6.116	62

Table 4.12 % Theoretical density of sintered modified BNLT samples

Composition	Measured density (g/cm ³)	Theoretical density (g/cm ³)	%Theoretical density
Sintered at 1100 °C, 2 h			
BNLT+Zr 0.5 at%	5.816	6.020	97
BNLT+Zr 1.0 at%	5.871	6.026	97
BNLT+Zr 1.5 at%	5.837	6.021	97
BNLT+Zr 2.0 at%	5.858	6.017	97
BNLT+Zr 2.5 at%	5.793	6.021	96
Sintered at 1050 °C, 2 h			
BNLT+Nb 0.5 at%	5.785	6.346	91
BNLT+Nb 1.0 at%	5.956	6.319	94
BNLT+Nb 1.5 at%	5.926	6.321	94
BNLT+Nb 2.0 at%	5.941	6.381	93
BNLT+Nb 2.5 at%	5.733	6.346	90
Sintered at 1100 °C, 2 h			
BNLT+Fe 0.5 at%	5.895	6.034	98
BNLT+Fe 1.0 at%	5.892	6.025	98
BNLT+Fe 1.5 at%	5.884	6.048	97
BNLT+Fe 2.0 at%	5.879	6.089	97
BNLT+Fe 2.5 at%	5.870	6.116	96

4.5 The phase transition by Differential Scanning Colorimetry

The phase transitions of modified $\text{Bi}_{0.5}\text{Na}_{0.485}\text{La}_{0.005}\text{TiO}_3$ were characterized by DSC technique. The sintered pellets were ground into fine particle sizes and annealed to reduce internal stress. Table 4.13 showed the phase transition temperatures of all samples and the results of phase transitions were shown in the Appendix. The phase transition which obtained by heat up of Zr modified BNLT at 0.5, 1.0, 1.5 and 2.0 at% Zr were 324, 259, 329 and 279 °C, respectively. For 2.5 at% Zr in BNLT did not observe any peak of phase transition over 25-450 °C of temperature. While cooling down, the phase transition of Zr modified BNLT shifted to the lower temperature and also for 2.5 at% Zr did not show any peaks all over the analysis temperature.

The phase transition of 0.5, 1.0, 1.5 and 2.0 at% Nb in BNLT system occurred at 318, 312, 308 and 295 °C, respectively. And 2.5 at% Nb in BNLT system did not show any peaks. The peak area of DSC curve represents the work per sample weight (J/g). The transition temperature of 0.5, 1.0, 1.5 and 2.0 at% Nb in BNLT system tend to decrease until 2.5 at% Nb where the DSC peak disappears. While cooling down; all of phase transitions of Nb-BNLTs were shifted to lower temperature.

The Fe modified BNLT system, the phase transitions while heating up of 0.5, 1.0, 1.5, 2.0 and 2.5 at% Fe were 320, 320, 317, 314 and 310 °C, respectively. For cooling down, the phase transition were also shifted to lower temperature which were 248, 254, 260, 266 and 269 °C of 0.5, 1.0, 1.5, 2.0 and 2.5 at% Fe, respectively.

For this section, it is concluded that the phase transition temperature of the modified BNLTs decreases with increasing in the substituent content both upon heating up and cooling down. For some compositions, phase transitions could not be observed by DSC technique.

Table 4.13 Phase transitions of the modified BNLTs

Compositions	Phase Transition temperature (°C)	
	Heating up	Cooling down
$\text{Bi}_{0.5}\text{Na}_{0.485}\text{La}_{0.005}\text{Zr}_x\text{Ti}_{(1-x)}\text{O}_3$		
x = 0.005	324.18	231.88
x = 0.010	258.68	-
x = 0.015	328.85	230.03
x = 0.020	279.39	228.38
x = 0.025	-	-
$\text{Bi}_{0.5}\text{Na}_{0.485}\text{La}_{0.005}\text{Nb}_x\text{Ti}_{(1-(5/4)x)}\text{O}_3$		
x = 0.005	317.99	245.84
x = 0.010	311.84	256.03
x = 0.015	307.67	261.04
x = 0.020	295.63	265.00
x = 0.025	-	-
$\text{Bi}_{0.5}\text{Na}_{0.485}\text{La}_{0.005}\text{Fe}_x\text{Ti}_{(1-(3/4)x)}\text{O}_3$		
x = 0.005	320.28	247.57
x = 0.010	320.02	253.61
x = 0.015	317.22	259.52
x = 0.020	314.01	266.25
x = 0.025	309.90	269.21

4.6 Microstructure Investigation

The microstructures of modified $\text{Bi}_{0.5}\text{Na}_{0.485}\text{La}_{0.005}\text{TiO}_3$ were investigated by SEM. The polished pellets of all samples were thermally etched at the 100°C below sintering temperatures [46]. The average grain size of BNLT and modified BNLT was performed using the line-intercept method and the result was summarized in Table 4.14 and Fig. 4.18. The SEM micrographs of pure BNLT and Zr-BNLT were shown in the Fig. 4.15 were performed the average grain size of 1 micron. The addition of Zr^{4+} content in BNLT compounds does not effect to the grain size of BNLT. The average grain size of Zr-BNLTs is approximately 1 micron. For Nb-BNLT, the microstructure of pure BNLT was affected by adding small amount of Nb. The SEM micrographs of Nb-BNLTs were shown in Fig. 4.16, it can clearly be observed that after the doping of the Nb^{5+} ions, the growth grain was significantly suppressed, yielding grain size of about three times (from 1 to 0.3 micron) smaller than those of the undoped BNLT ceramics. Increasing in the content of Nb^{5+} up to 2.5 at% Nb in BNLT compounds the microstructure become to sharp edge of grain.

For Fe-BNLT, the grain size is increased with the addition of Fe^{3+} content in the system. The average grain size of 0.5, 1.0, 1.5, 2.0 and 2.5 at% Fe^{3+} are 1.13, 1.46, 2.21, 3.41 and 4.23 microns, respectively. The SEM micrographs of Fe-BNLTs were shown in Fig. 4.17.

For this section, it concluded that Nb dopant affected the grain size of BNLT system by reducing grain size of BNLT from 1 micron into 0.3 micron. Concentration of Nb substituent is insignificant in grain size of modified BNLT. Fe dopant increased the grain size in BNLT system from 1 to 4 micron. It could be concluded that the addition of Nb restrained the grain growth of the ceramics materials and the addition of Fe^{3+} is a grain growth promoter of the BNLT ceramics.

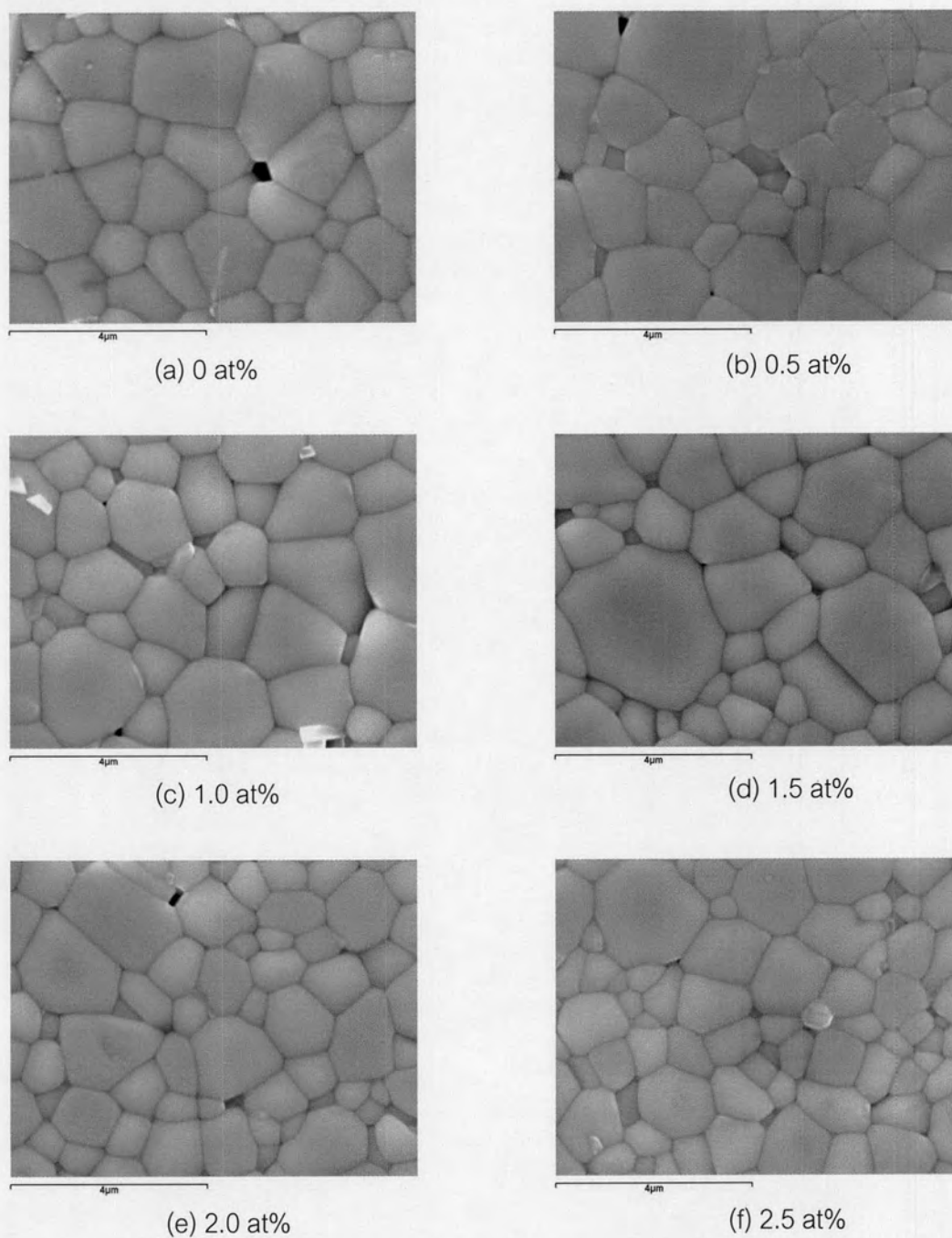


Fig. 4.15 Microstructure (x15000) of the modified BNLt with Zr additives sintered at 1100 °C for 2 hrs: (a) 0 at%, (b) 0.5 at%, (c) 1.0 at%, (d) 1.5 at%, (e) 2.0 at%, and (f) 2.5 at%

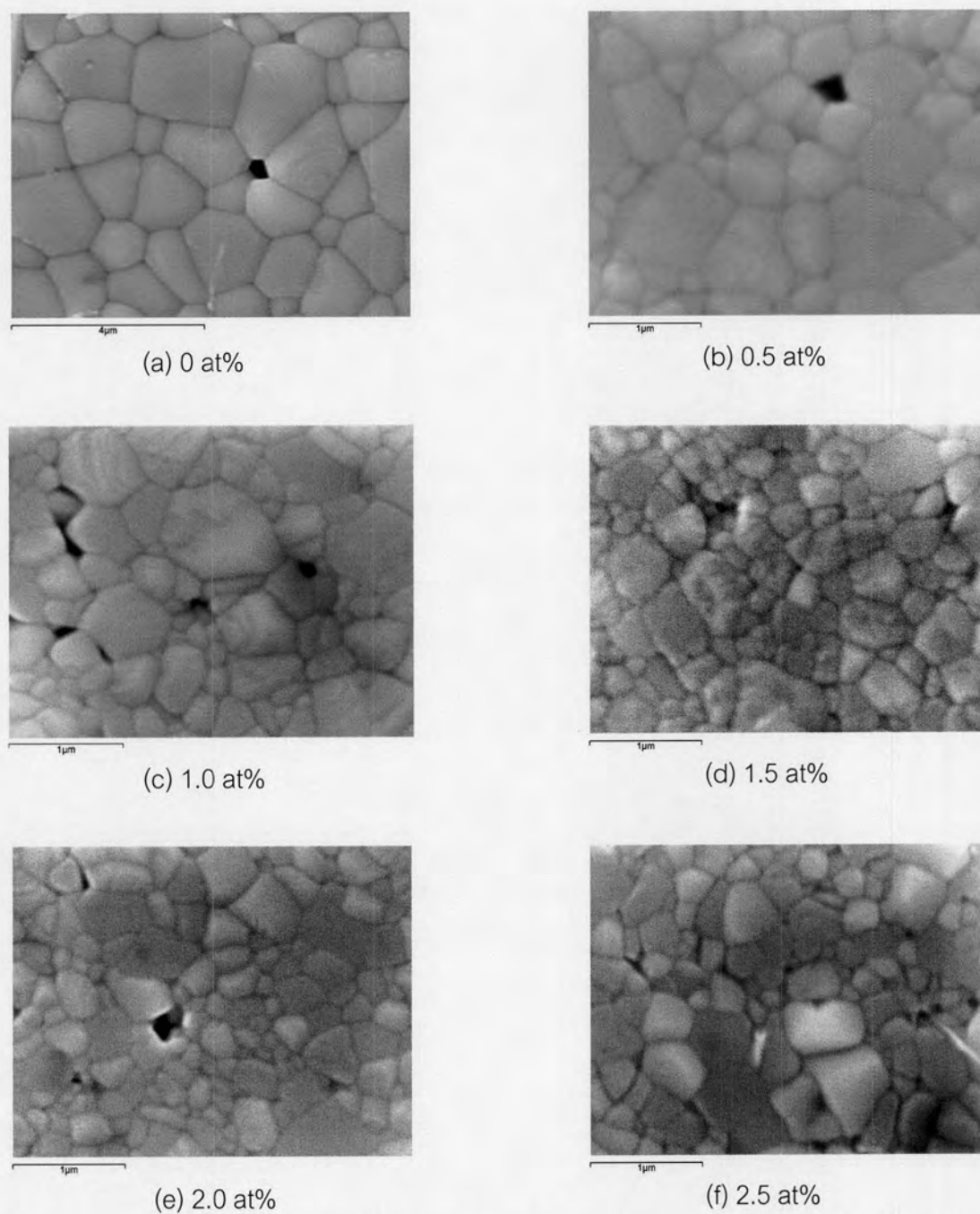


Fig. 4.16 Microstructure (x35000) of the modified BNLT with Nb additives sintered at 1050 °C for 2 hrs compare with pure BNLT (x15000) sintered at 1100 °C for 2 hrs: (a) 0 at%, (b) 0.5 at%, (c) 1.0 at%, (d) 1.5 at%, (e) 2.0 at%, and (f) 2.5 at%

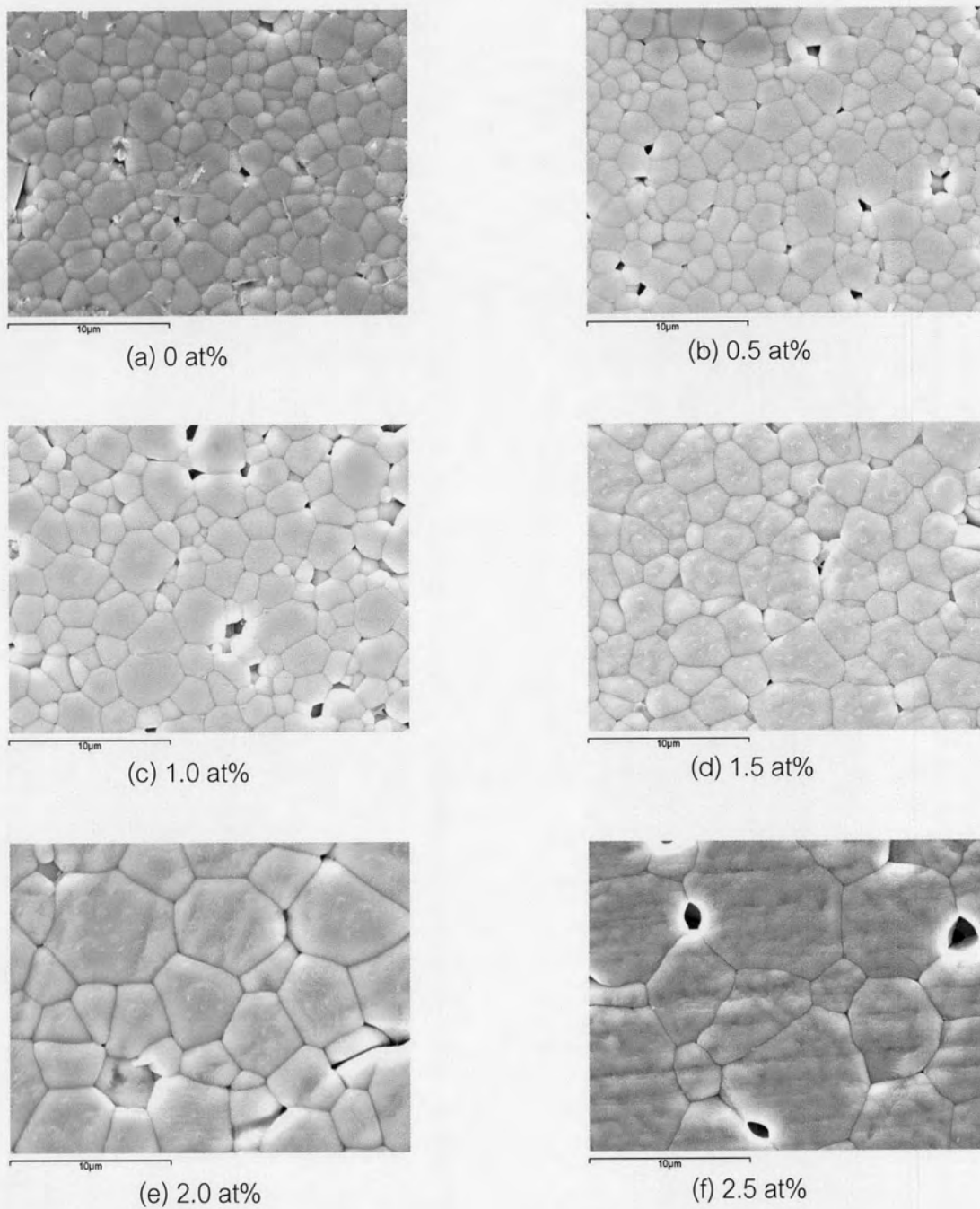


Fig. 4.17 Microstructure (x5000) of the modified BNLT with Fe additives sintered at 1100 °C for 2 hrs: (a) 0 at%, (b) 0.5 at%, (c) 1.0 at%, (d) 1.5 at%, (e) 2.0 at%, and (f) 2.5 at%

Table 4.14 The average grain size of the BNLT and modified BNLTs

Composition	Range of grain size (micron)	Average of grain size (micron)
BNLT	0.79 - 1.25	1.01 ± 0.08
BNLT+0.5%Zr	0.77 - 1.70	1.06 ± 0.08
BNLT+1.0%Zr	0.86 - 1.38	1.09 ± 0.09
BNLT+1.5%Zr	0.68 - 1.38	1.06 ± 0.11
BNLT+2.0%Zr	0.62 - 1.18	0.88 ± 0.02
BNLT+2.5%Zr	0.62 - 1.14	0.81 ± 0.04
BNLT+0.5%Nb	0.33 - 0.63	0.44 ± 0.03
BNLT+1.0%Nb	0.27 - 0.41	0.34 ± 0.01
BNLT+1.5%Nb	0.27 - 0.44	0.33 ± 0.03
BNLT+2.0%Nb	0.22 - 0.45	0.32 ± 0.03
BNLT+2.5%Nb	0.24 - 0.45	0.30 ± 0.03
BNLT+0.5%Fe	0.83 - 1.49	1.13 ± 0.11
BNLT+1.0%Fe	1.03 - 2.06	1.46 ± 0.19
BNLT+1.5%Fe	1.66 - 2.48	2.21 ± 0.22
BNLT+2.0%Fe	2.21 - 4.93	3.41 ± 0.38
BNLT+2.5%Fe	3.10 - 6.22	4.23 ± 0.24

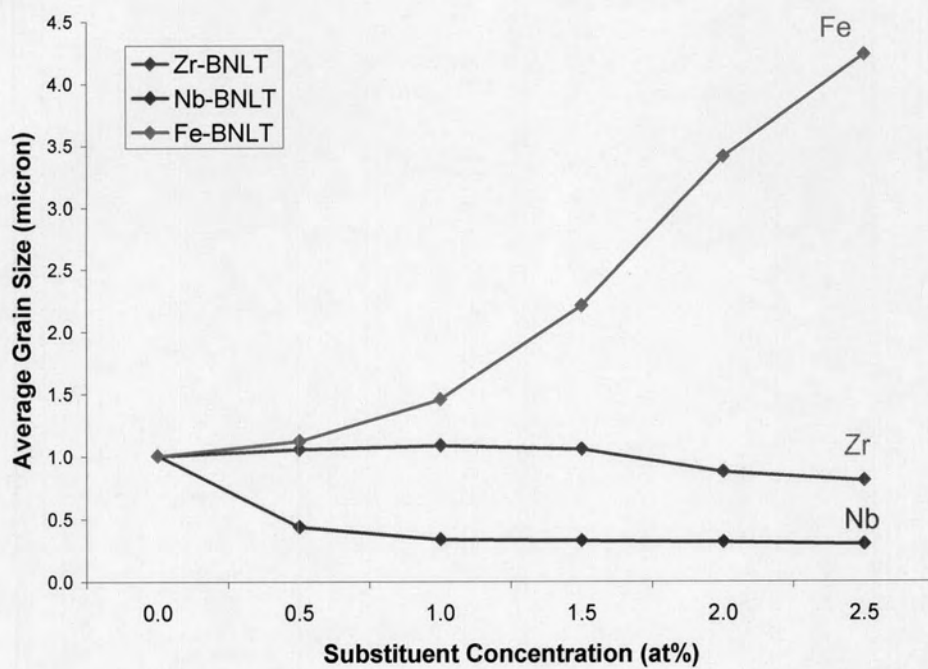
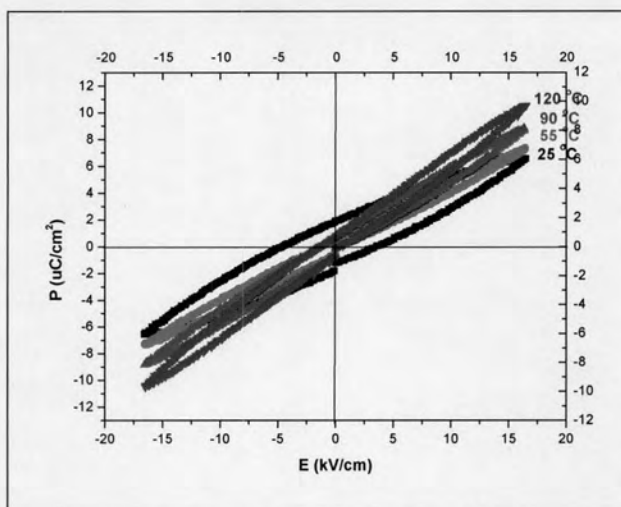


Fig. 4.18 The plots between average grain size and substituent concentrations

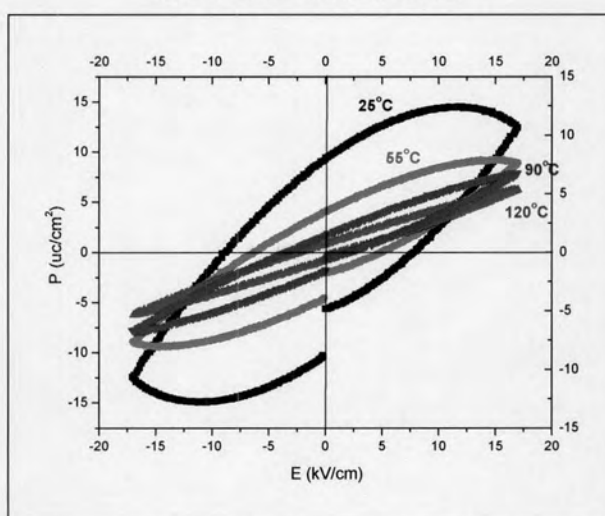
4.7 Polarization measurement

The polarizations of all samples were conducted by Hysteresis analyzer, RT66A, at various temperatures (25, 55, 90 and 120 °C) (Fig. 4.19). For Zr-BNLT, the plot between polarization (P) and electric field (E) loop or P-E loop presented in different slope with various measurement temperature. The slope of P-E loop is presented as a dielectric permittivity that equal to the polarization (P) by the electric field (E) [36, 47]. The slope of P-E loop or the dielectric permittivities of Zr-BNLT samples is increased with an increasing of measured temperature. The Zr^{4+} content affected directly with the remanent polarization. The addition Zr^{4+} content presented lower the remanent polarization. 0.5 at% of Zr^{4+} showed the highest remanent polarization at 25 °C ($1.9 \mu\text{C}/\text{cm}^2$) compare with the other Zr concentrations. The P-E loops and polarization properties of Zr-BNLTs were shown in Fig. 4.20 and Table 4.15. For Nb-BNLT, the 0.5 and 2.5 at% of Nb^{5+} have low density ($<93\%D_{th}$) accompanied with high dielectric loss (14 and 26%, respectively) so the P-E loops presented the swell loops with containing lossy effect. The 1.0, 1.5 and 2.0 at % of Nb^{5+} presented higher remanent polarization compare with Zr-BNLT ones. Nb doped in BNLTs obtained softer hysteresis loop like Nb doped in PZT [47]. The 2.0 at% of Nb^{5+} presented the highest remanent polarization which is $20.1 \mu\text{C}/\text{cm}^2$. The P-E loops and polarization properties of Nb-BNLTs were shown in Fig. 4.21 and Table 4.15. For Fe-BNLT, the P-E loop presented in slim shape all the ranges of the Fe^{3+} concentration. 2.5 at% Fe^{3+} showed the highest remanent polarization which is $1.0 \mu\text{C}/\text{cm}^2$. The P-E loops and polarization properties of Fe-BNLTs were shown in Fig. 4.22 and Table 4.15.

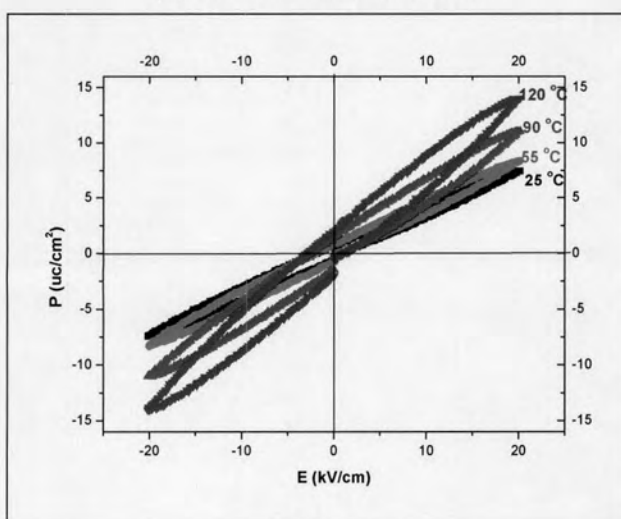
The conclusion of this section is the P-E loop of Zr- and Fe-BNLT were presented the slim loops which exhibiting field-enforced ferroelectric (SFE) behavior [8]. The remanent polarization was decreased with an increasing in the Zr concentration. The Zr doped in BNLT system behaves as a hard doping [36]. The 1.0 – 2.0 at% Nb doped in BNLT system is increasing the remanent polarization like soft doping and change the hysteresis to softer hysteresis loop. Yet the 0.5 and 2.5 at% Nb posses high porosity and dielectric loss due to the lossy effect of hysteresis loops.



(a) Zr-BNLT at 0.5 at%Zr

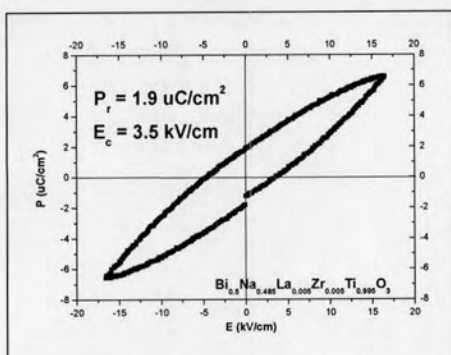


(b) Nb-BNLT at 1.0 at%Nb

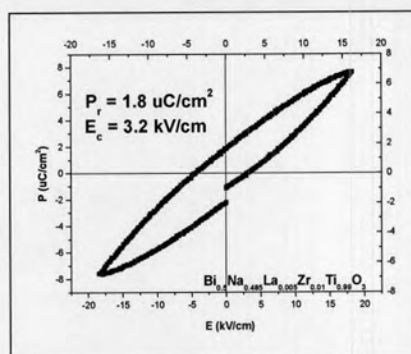


(c) Fe-BNLT at 0.5 at%Fe

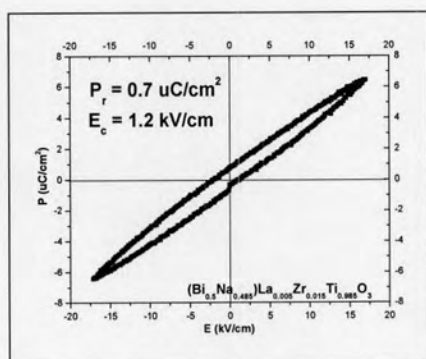
Fig. 4.19 P-E loops of modified BNLT at 25, 55, 90 and 120 °C; (a) 0.5 at% Zr in BNLT, (b) 1.0 at% Nb in BNLT and (c) 0.5 at% Fe in BNLT



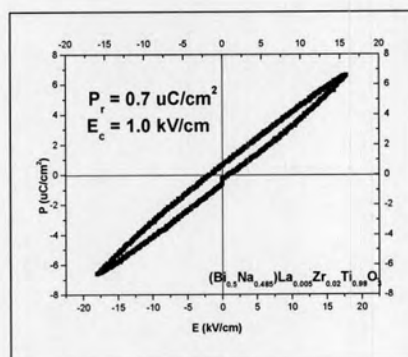
(a) 0.5 at%



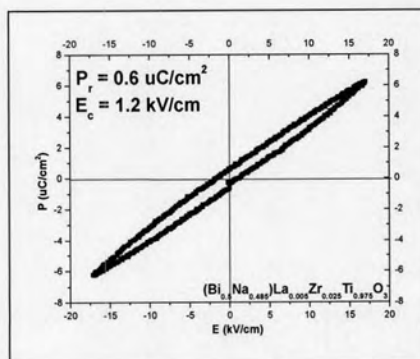
(b) 1.0 at%



(c) 1.5 at%

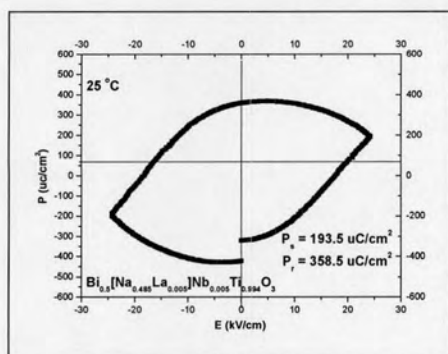


(d) 2.0 at%

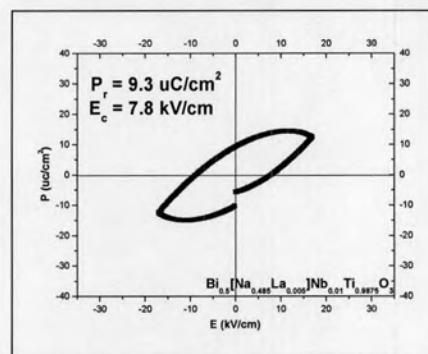


(e) 2.5 at%

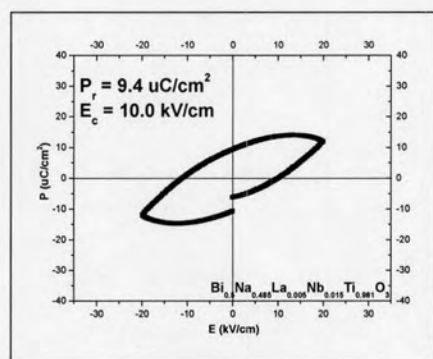
Fig. 4.20 P-E loop of Zr-BNLT at 25 °C; (a) 0.5 at%, (b) 1.0 at%, (c) 1.5 at%, (d) 2.0 at% and (e) 2.5 at%



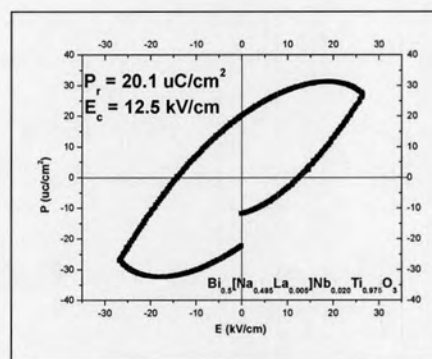
(a) 0.5 at%



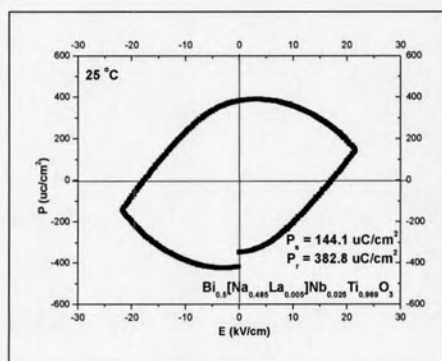
(b) 1.0 at%



(c) 1.5 at%

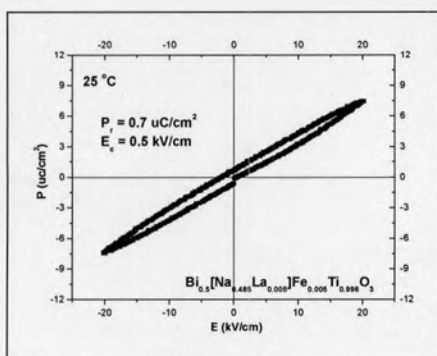


(d) 2.0 at%

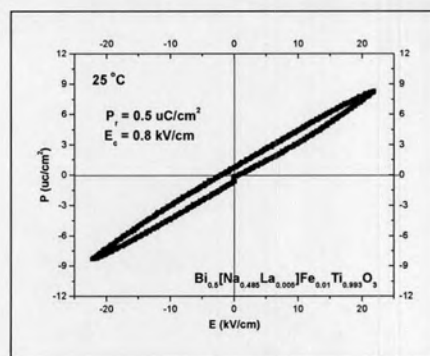


(e) 2.5 at%

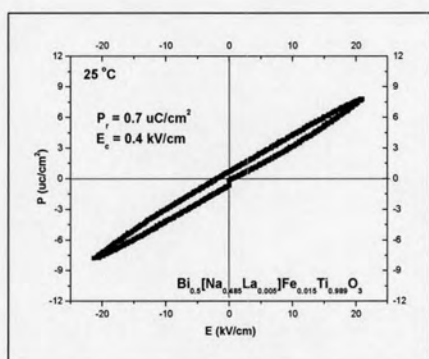
Fig. 4.21 P-E loop of Nb-BNLT at 25 °C; (a) 0.5 at%, (b) 1.0 at%, (c) 1.5 at%, (d) 2.0 at% and (e) 2.5 at%



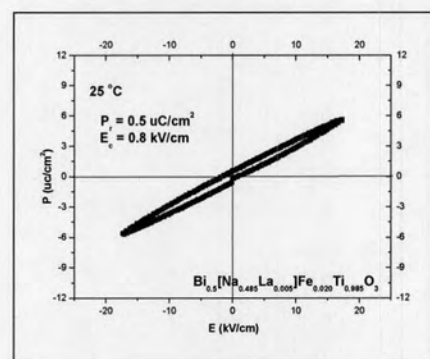
(a) 0.5 at%



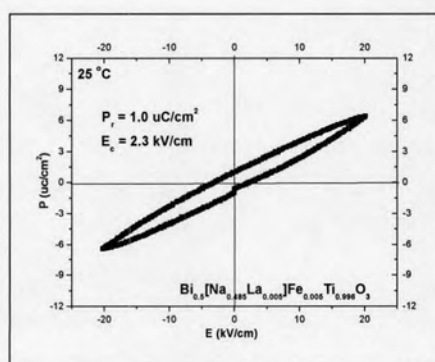
(b) 1.0 at%



(c) 1.5 at%



(d) 2.0 at%



(e) 2.5 at%

Fig. 4.22 P-E loop of Fe-BNLT at 25 °C; (a) 0.5 at%, (b) 1.0 at%, (c) 1.5 at%, (d) 2.0 at% and (e) 2.5 at%

Table 4.15 The results of Polarization Measurement

Compositions	Remanent Polarization ($\mu\text{C}/\text{cm}^2$)	Saturated Polarization ($\mu\text{C}/\text{cm}^2$)	Coercive Field (kV/cm)
$\text{Bi}_{0.5}\text{Na}_{0.485}\text{La}_{0.005}\text{Zr}_x\text{Ti}_{(1-x)}\text{O}_3$			
$x = 0.005$	1.9	6.6	3.5
$x = 0.010$	1.8	7.6	3.2
$x = 0.015$	0.7	6.4	1.2
$x = 0.020$	0.7	7.3	1.0
$x = 0.025$	0.6	5.9	1.2
$\text{Bi}_{0.5}\text{Na}_{0.485}\text{La}_{0.005}\text{Nb}_x\text{Ti}_{(1-(5/4)x)}\text{O}_3$			
$x = 0.005$	358.5	193.5	23.5
$x = 0.010$	9.3	12.4	7.8
$x = 0.015$	9.4	12.0	10.0
$x = 0.020$	20.1	27.0	12.5
$x = 0.025$	382.8	144.1	3.0
$\text{Bi}_{0.5}\text{Na}_{0.485}\text{La}_{0.005}\text{Fe}_x\text{Ti}_{(1-(3/4)x)}\text{O}_3$			
$x = 0.005$	0.7	7.2	0.5
$x = 0.010$	0.5	7.9	0.8
$x = 0.015$	0.7	7.8	0.4
$x = 0.020$	0.5	5.6	0.8
$x = 0.025$	1.0	6.4	2.3

4.9 Dielectric Properties

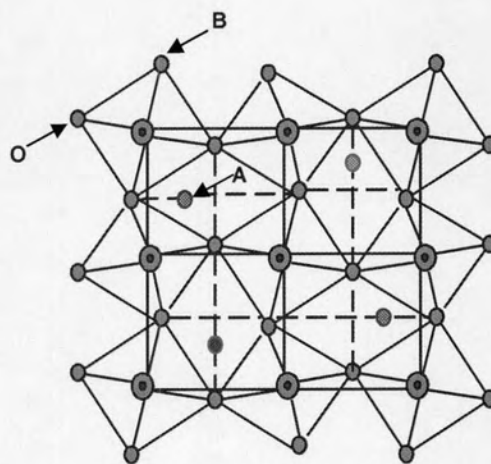
The dielectric constant (relative permittivities) and dissipation factors (dielectric loss) of all samples were performed both of unpoled and poled specimens at the frequency of 1, 10, 100 kHz and 1 MHz. Table 4.16-4.17 presents the dielectric constants and dissipation factors of the modified BNLT. It was found that the dielectric constant of both poled and unpoled samples tend to decreased while the measuring frequencies increased. There are 4 mechanisms of polarization which are electronic polarization, atomic polarization, dipolar polarization and space charge polarization which was mentioned in Chapter II. The affected of Electronic polarization that occurred at very high frequency, was dominated by the movement of the electron cloud. At the lower frequencies, the atomic polarization, dipolar and space charge polarization will play the parts rather than the previous one. The Zr-BNLT could not be poled, so the permittivities and dissipation factors were obtained only for unpoled samples. The value of dielectric permittivities of 0.5- 2.0 at% are in the range of 630-680 and 2.5 at% Zr presented 870 of dielectric permittivity with accompanied of high dissipation factor (32%). The dissipation factors of 0.5-2.0 at% Zr are in the range of 4-5%. The plots of dielectric permittivities and dissipation factors versus Zr concentration were shown in Fig. 4.24. The dielectric constants of Zr doped BNLT are slightly higher than Nb- and Fe-BNLT. This phenomenon may result from the difference in the microstructure. The grain size of Zr-BNLTs is approximately 1 micron, indicating that the domain walls were clamped and not free to move. The internal stresses generated by the clamped domain walls contribute to an increase in the permittivity which is proportional to a high value of dielectric constant [8].

For Nb-BNLT, the dielectric permittivities and dissipation factors of unpoled specimens of 0.5, 1.0, 1.5, 2.0 and 2.5 at% Nb are 610, 520, 560, 570 and 733, respectively, and dissipation factors are 14%, 5%, 9%, 9% and 26%, respectively. Although the Nb-modified BNLT specimens possessed small grains of approximately 0.3 micron, their permittivity at room temperature was low compared with Zr-BNLT. This may affect from the difference of the distortion. For perovskite structure, there are two types of distortions which are packing distortion (Fig. 4.23 (a)) and off-center distortion (Fig. 4.23 (b)). Packing

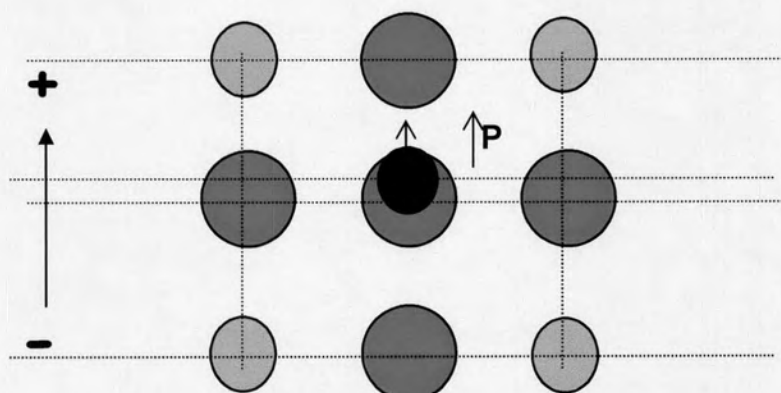
distortion is the main distortion in general BNT system. For B-site modification of BNLT system, the off-center distortion becomes dominate because the Nb dopant is substituted in Ti-site and changed the bonding strength of Ti-O into Nb-O and probably changed in individual dipole moment resulting to the low value of the fine-grained Nb-modified BNLT [5]. For poled specimens, the dielectric permittivities and dissipation factors of 0.5, 1.0, 1.5, 2.0 and 2.5 at% Nb are 710, 550, 530, 590 and 750 respectively, and dissipation factors are 24, 6, 10, 10 and 22%. For 0.5 and 2.5 at% of Nb doped BNLT contains high porosity which showed high dissipation factor. The plots of dielectric permittivities and dissipation factors versus Nb concentration were shown in Fig. 4.25.

For Fe-BNLT system, the dielectric permittivities are in the range of 570-670 and tend to decrease with increasing of Fe concentration. The lower of dielectric constant of Fe-BNLT system compared with Zr-BNLT system may result from coarse-grained of Fe modified BNLT system. The grain size of Fe-BNLT system was increased with an increasing amount of Fe. The larger grain possessed a lower dielectric constant at room temperature same as the dielectric properties of BaTiO_3 in that the coarse-grained BaTiO_3 ceramic has a low dielectric constant at room temperature [47]. The maximum dielectric permittivity is 1.0 at% of Fe (665). The dissipation factors of all range of Fe concentration are 4%. The plots of dielectric permittivities and dissipation factors versus Fe concentration were shown in Fig. 4.26.

To summarize, the dielectric constant of modified BNLT system is sensitive to composition, microstructure and measurement frequency. Therefore, the dielectric properties of BNLT can be modified by taking an advantage in controlling these factors.



(a) packing distortion



(b) Off-center distortion

Fig. 4.23 Two kinds of distortion from the ideal perovskite structure: (a) packing distortion and (b) off-center distortion [5]

Table 4.16 The dielectric permittivities and dissipation factors of unpoled-modified BNLT samples

Compositions	1kHz		10kHz		100kHz		1MHz	
	K	DF	K	DF	K	DF	K	DF
$\text{Bi}_{0.5}\text{Na}_{0.485}\text{La}_{0.005}\text{Zr}_x\text{Ti}_{(1-x)}\text{O}_3$ Sintered at 1100°C, 2 h								
x = 0.005	729	4.2%	686	4.3%	642	4.8%	599	5.9%
x = 0.010	721	4.2%	679	4.3%	636	4.8%	592	6.0%
x = 0.015	726	4.0%	684	4.2%	641	4.7%	598	5.9%
x = 0.020	724	4.0%	682	4.2%	640	4.7%	597	6.0%
x = 0.025	721	3.9%	696	4.2%	638	4.7%	595	5.9%
$\text{Bi}_{0.5}\text{Na}_{0.485}\text{La}_{0.005}\text{Nb}_x\text{Ti}_{(1-(5/40)x)}\text{O}_3$ Sintered at 1050°C, 2 h								
x = 0.005	612	14.0%	542	6.9%	505	4.9%	472	5.5%
x = 0.010	519	4.9%	489	4.2%	459	4.4%	430	5.3%
x = 0.015	562	8.7%	516	5.2%	483	4.7%	452	5.4%
x = 0.020	567	8.7%	516	5.7%	481	4.7%	450	5.3%
x = 0.025	733	26.0%	561	14.3%	480	8.0%	440	6.2%
$\text{Bi}_{0.5}\text{Na}_{0.485}\text{La}_{0.005}\text{Fe}_x\text{Ti}_{(1-(3/4)x)}\text{O}_3$ Sintered at 1100°C, 2 h								
x = 0.005	614	4.2%	577	4.4%	541	4.7%	504	5.7%
x = 0.010	665	4.2%	625	4.5%	585	4.8%	544	6.2%
x = 0.015	652	4.2%	612	4.5%	573	4.8%	534	5.6%
x = 0.020	599	4.3%	562	4.5%	525	4.8%	489	5.7%
x = 0.025	570	4.4%	534	4.5%	499	4.8%	464	49.8%

K – dielectric constant, $\tan \delta$ - dissipation factor

Table 4.17 The dielectric permittivities and dissipation factors of poled-modified BNLT samples

Compositions	1kHz		10kHz		100kHz		1MHz	
	K	DF	K	DF	K	DF	K	DF
$\text{Bi}_{0.5}\text{Na}_{0.485}\text{La}_{0.005}\text{Zr}_x\text{Ti}_{(1-x)}\text{O}_3$ Sintered at 1100°C, 2H x = 0.005 x = 0.010 x = 0.015 x = 0.020 x = 0.025	-	-	-	-	-	-	-	-
$\text{Bi}_{0.5}\text{Na}_{0.485}\text{La}_{0.005}\text{Nb}_x\text{Ti}_{(1-(5/40)x)}\text{O}_3$ Sintered at 1050°C, 2H x = 0.005 x = 0.010 x = 0.015 x = 0.020 x = 0.025	710	24%	539	6.5%	503	4.9%	470	5.5%
$\text{Bi}_{0.5}\text{Na}_{0.485}\text{La}_{0.005}\text{Fe}_x\text{Ti}_{(1-(3/4)x)}\text{O}_3$ Sintered at 1100°C, 2H x = 0.005 x = 0.010 x = 0.015 x = 0.020 x = 0.025	274	3.9%	245	4.3%	245	4.3%	230	5.5%
	464	3.5%	419	4.1%	419	4.1%	393	5.1%
	515	3.8%	464	4.2%	464	4.2%	435	6.6%
	475	3.7%	435	3.6%	435	3.6%	412	5.1%
	377	3.1%	346	3.5%	346	3.5%	331	4.5%

K – dielectric constant, $\tan \delta$ – dissipation factor

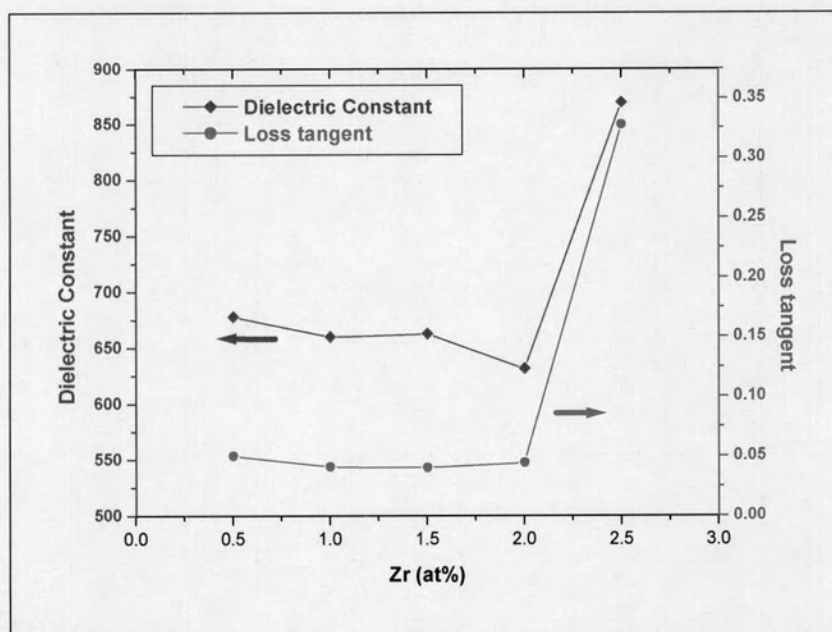
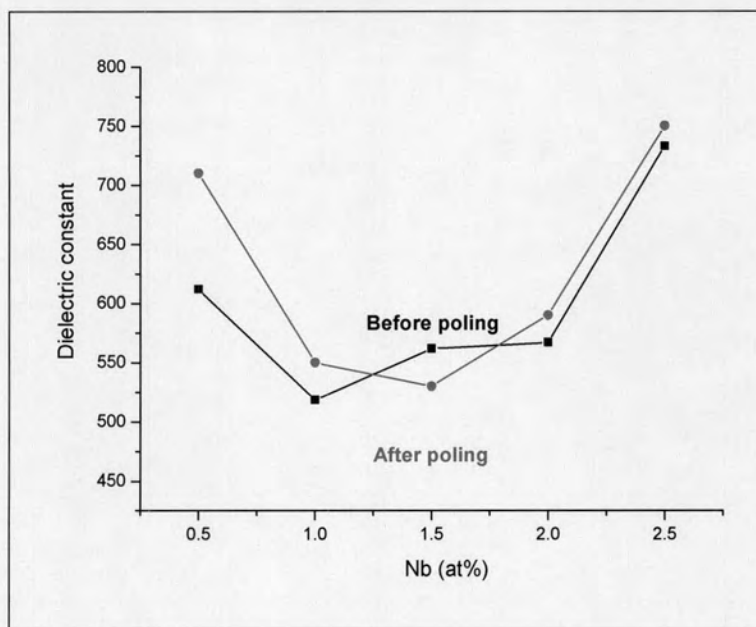
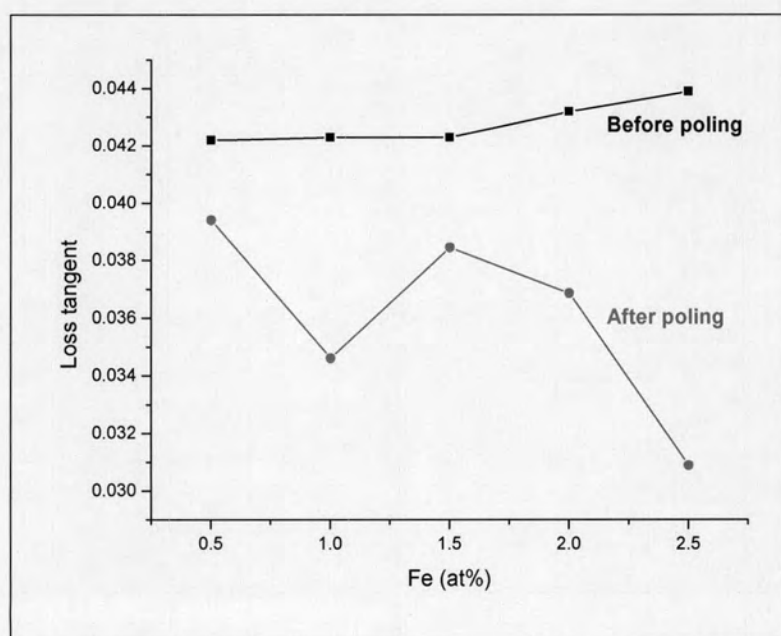


Fig. 4.24 The plots of dielectric permittivities and dissipation factors versus Zr concentration

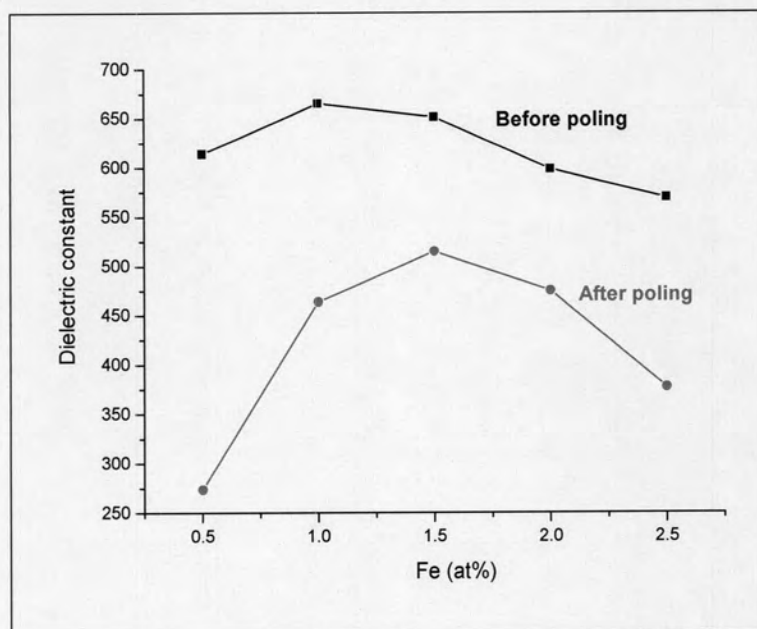


(a) Dielectric permittivity

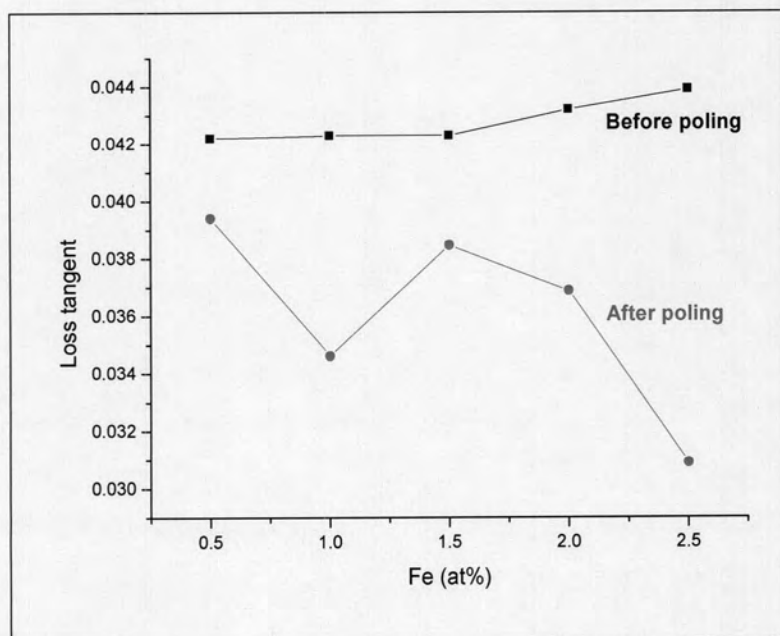


(b) Loss tangent

Fig. 4.25 The plots of dielectric permittivities and dissipation factors versus Nb concentration; (a) Dielectric permittivity, (b) Loss tangent



(a) Dielectric permittivity

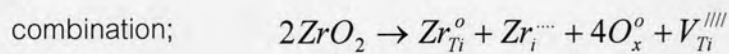
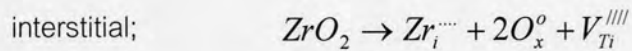
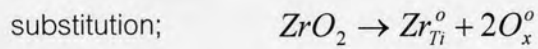


(b) Loss tangent

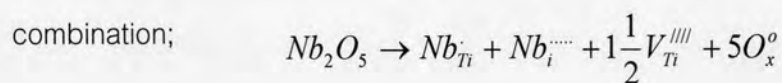
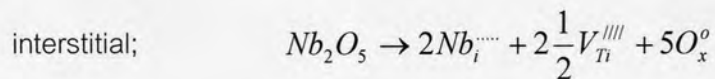
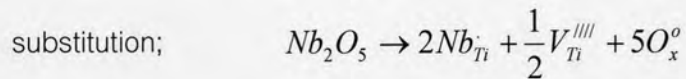
Fig. 4.26 The plots of dielectric permittivities and dissipation factors versus Fe concentration; (a) Dielectric permittivity, (b) Loss tangent

4.10 Volume Resistivity

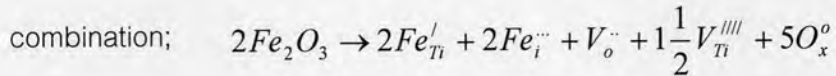
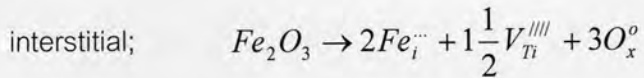
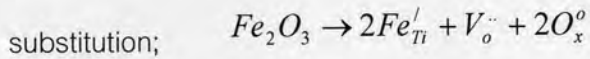
Volume resistivities of all of samples were determined the by a Resistivity Chamber (Keithley Model 6150) at room temperature (23-25 °C). The volume resistivities of all samples were shown in Table 4.18. The volume resistivity of pure BNLT is 2.33×10^{13} ohm.cm. The Zr doped BNLT abnormally 6 orders of magnitude decreases from the pure BNLT that might be affected from internal defect showed as possible reactions [25] below;



For Nb doped BNLT, the volume resistivity of 1.0, 1.5 and 2.0 at% Nb are in the order of 10^9 to 10^{10} ohm.cm, and 0.5 and 2.5 at% which are lower density ($<93\%D_{th}$) than another compositions that contains more porosity and obtained lesser in volume resistivity. The possible reactions of Nb doped in the BNLT system showed as equations below;



For Fe doped BNLT, the volume resistivity are not much different from the pure BNLT ones. The volume resistivities are in order of 10^{10} to 10^{11} and the possible reactions of Fe doped in the BNLT system showed as below;



This section can be concluded that the Zr doped BNLTs were 6 orders reduced the volume resistivity from the pure BNLT by created Ti vacancies also like the Nb doped BNLTs which 2-3 orders decreased from the undoped BNLT. Ti vacancies creations in Zr and Nb doped BNLT ceramic posses n-type conductivity [48].

For Fe doped in BNLT created oxygen vacancies in the lattice and shown as a p-type conductivity. The perovskite structure is composed of oxygen octahedral, and it has a limitation of Fe content in BNLT system which should be lower a certain limit in order to maintain the stability of the oxygen octahedral framework [48]. The vacancies which are created in the BNLT system also decrease the volume resistivity, so the poling process will difficult to success.

4.11 Piezoelectric Properties

In this section, the modified BNLT compositions are discussed in terms of their piezoelectric properties, i.e., the piezoelectric coefficient (d_{33}) and electromechanical coupling factors (k_p and k_t). The d_{33} constants were directly measured whereas the electromechanical coupling factors were calculated from the resonance and antiresonance frequencies. The poling process was conducted with Zr-BNLT, Nb-BNLT and Fe-BNLT systems at the 45 kV/cm of poling field. Regarding to low volume resistivity of Zr doped in BNLT ceramics, so the modified BNLT with Zr substitution could not be poled and tested for piezoelectric properties. The piezoelectric properties of Nb-BNLT and Fe-BNLT were summarized in Table 4.19. The 0.5, 1.0, 1.5, 2.0 and 2.5 at% Nb exhibited the d_{33} values approximately 39, 43, 31, 29 and 40 pC/N, respectively. All the k_p and k_t values of each

Table 4.18 The volume resistivity of modified BNLT

Compositions	volume resistivity (ohm.cm)
BNLT	2.33×10^{13}
BNLT+0.5%Zr	1.49×10^7
BNLT+1.0%Zr	2.52×10^7
BNLT+1.5%Zr	6.47×10^7
BNLT+2.0%Zr	6.51×10^7
BNLT+2.5%Zr	4.03×10^7
BNLT+0.5%Nb	4.58×10^8
BNLT+1.0%Nb	1.43×10^{10}
BNLT+1.5%Nb	8.67×10^9
BNLT+2.0%Nb	9.26×10^9
BNLT+2.5%Nb	4.51×10^8
BNLT+0.5%Fe	1.96×10^{11}
BNLT+1.0%Fe	5.25×10^{11}
BNLT+1.5%Fe	7.05×10^{10}
BNLT+2.0%Fe	1.99×10^{10}
BNLT+2.5%Fe	1.62×10^{10}

compositions were in the range of 11-13% and 45-48%, respectively. The maximum of the d_{33} value of Nb doped BNLT is approximately 43 pC/N which is present in 1.0 at% Nb. The 0.5, 1.0, 1.5, 2.0 and 2.5 at% Fe exhibited the d_{33} value approximately 133, 155, 142, 146 and 135 pC/N, respectively. All the k_p and k_t values of each compositions were in the range of 12-17% and 45-48%, respectively. The maximum of the d_{33} value of Fe doped BNLT is approximately 155 pC/N which is presented in 1.0 at% Fe.

The isovalent and aliovalent substitutions caused high values of dielectric constant and dissipation factor of the modified-BNLT compositions. This could result from several factors. First is the microstructure. Second is the difference in distortion occurring and third is the defects derived from these substituents. Defects from substitution could alter the piezoelectric properties of the modified BNLT compositions as well.

Table 4.19 The piezoelectric properties of Nb-BNLTs and Fe-BNLTs

Compositions	d_{33} (pC/N)	g_{33} (pC/N)	$d_{33}g_{33}$	k_t (%)	k_p (%)	N_t (Hz.mm)	N_p (Hz.mm)
BNLT + 0.5 at% Nb	39	6	243	45	12	2340	2921
BNLT + 1.0 at% Nb	43	11	419	46	13	2248	2819
BNLT + 1.5 at% Nb	31	7	210	49	12	2373	2922
BNLT + 2.0 at% Nb	29	5	147	48	11	2437	2955
BNLT + 2.5 at% Nb	40	6	243	48	12	2418	2988
BNLT + 0.5 at% Fe	133	55	134	45	15	2453	3235
BNLT + 1.0 at% Fe	155	38	0	46	17	2509	3222
BNLT + 1.5 at% Fe	142	31	148	49	12	1258	2787
BNLT + 2.0 at% Fe	146	36	0	48	12	1197	3302
BNLT + 2.5 at% Fe	135	40	139	48	15	2403	3123

Dielectric and piezoelectric properties of all samples were measured at 1 kHz

4.12 Summary

The isovalent and aliovalent substitutions were employed in the development of the bismuth sodium lanthanum titanate ($\text{Bi}_{0.5}\text{Na}_{0.485}\text{La}_{0.005}\text{TiO}_3$: BNLT) compositions. Three chemical formulas are as listed: (a) $\text{Bi}_{0.5}\text{Na}_{0.485}\text{La}_{0.005}\text{Zr}_x\text{Ti}_{(1-x)}\text{O}_3$, (b) $\text{Bi}_{0.5}\text{Na}_{0.485}\text{La}_{0.005}\text{Nb}_x\text{Ti}_{(1-(5/4)x)}\text{O}_3$ and $\text{Bi}_{0.5}\text{Na}_{0.485}\text{La}_{0.005}\text{Fe}_x\text{Ti}_{(1-(3/4)x)}\text{O}_3$. Since the source of substituents was in the oxide form. The conventionally mixed oxide method was selected to prepare the mixed oxide powder. The 800°C for 2 hrs of sintering temperature were selected to performed the pure perovskite phase. To determining for the suitable sintering temperature of Zr-BNLT, Nb-BNLT and Fe-BNLT were conducted at 1100, 1050 and 1100°C for 2 hrs. The physical, electrical, dielectric and piezoelectric properties were summarized in Table 4.23. The excellent piezoelectric properties found within the Fe-modified BNLT system, combined with the comparative ease of processing and sintering, lead to an expectation in utilizing these compositions for lead-based compounds provide alternative materials for practical use in many applications such as transducer.. Moreover, they can be employed to subsidize the environmental problem due to the use of lead.

Table 4.23 Dielectric, Electrical and Piezoelectric properties of modified BNLT

Compositions	Before poling process		After poling process		volume resistivity (ohm.cm)	d_{33} (pC/N)	g_{33} (pC/N)	$d_{33}g_{33}$	k_t (%)	k_p (%)	N_t (Hz.mm)	N_p (Hz.mm)
	K	$\tan \delta$ (%)	K	$\tan \delta$ (%)								
$\text{Bi}_{0.5}\text{Na}_{0.485}\text{La}_{0.005}\text{Zr}_x\text{Ti}_{(1-x)}\text{O}_3$												
x = 0.005	729	4	-	-	1.49×10^7	-	-	-	-	-	-	-
x = 0.010	721	4	-	-	2.52×10^7	-	-	-	-	-	-	-
x = 0.015	726	4	-	-	6.47×10^7	-	-	-	-	-	-	-
x = 0.020	724	4	-	-	6.51×10^7	-	-	-	-	-	-	-
x = 0.025	721	4	-	-	4.03×10^7	-	-	-	-	-	-	-
$\text{Bi}_{0.5}\text{Na}_{0.485}\text{La}_{0.005}\text{Nb}_x\text{Ti}_{(1-(5/4)x)}\text{O}_3$												
x = 0.005	612	14	715	24	4.58×10^8	39	6	243	29	12	2340	2921
x = 0.010	519	5	452	6	1.43×10^{10}	43	11	419	27	13	2248	2819
x = 0.015	562	9	528	10	8.67×10^9	31	7	210	20	12	2373	2922
x = 0.020	567	9	573	10	9.26×10^9	29	5	147	20	11	2437	2955
x = 0.025	733	26	752	10	4.51×10^8	40	6	243	40	12	2418	2988
$\text{Bi}_{0.5}\text{Na}_{0.485}\text{La}_{0.005}\text{Fe}_x\text{Ti}_{(1-(3/4)x)}\text{O}_3$												
x = 0.005	614	4	274	4	1.96×10^{11}	133	55	7333	45	15	2453	3235
x = 0.010	665	4	464	3	5.25×10^{11}	155	38	5853	46	17	2509	3222
x = 0.015	652	4	515	4	7.05×10^{10}	142	31	4439	49	12	1258	2787
x = 0.020	599	4	475	4	1.99×10^{10}	146	36	5160	48	12	1197	3302
x = 0.025	570	4	377	3	1.62×10^{10}	135	40	5429	48	15	2403	3123

Dielectric and piezoelectric properties were measured at 1 kHz